Living with high potassium: an asset or a hindrance

Pramod Pantha[1], Dong-Ha Oh[1], David Longstreth[1] and Maheshi Dassanayake[1,*]

[1]Department of Biological Sciences, Louisiana State University, Baton Rouge, LA 70803, USA

*Address correspondence to: maheshid@lsu.edu

Abstract

K is more toxic than Na at similar concentrations but the molecular mechanisms governing excess K-induced salt stress responses, including excess K^+ signaling and major cellular functions interrupted during K toxicity in plants are unknown. We used *Arabidopsis thaliana* and its extremophyte relative *Schrenkiella parvula*, to explore this interesting but vastly unexplored question using comparative physiological, ionomic, transcriptomic, and metabolomic approaches aimed at understanding how plants can develop resilience to excess K toxicity. Our results showed that the stress responses exhibited by the two plants diverged at a decisive step where the stress-sensitive *A. thaliana* could not limit excess K influx and suffered severe nutrient depletion. The stress adapted model, *S. parvula*, was able to independently regulate reduction in K uptake while sustaining uptake of other major nutrients including N. Upheld N uptake and uninterrupted assimilation into primary metabolites allowed *S. parvula* to sustain growth and concurrently boost its antioxidant capacity and osmolyte pools, facilitated by a targeted transcriptomic response. In contrast, *A. thaliana* descended into mismanaged transcriptional cascades including induction of both biotic and abiotic stress responses and autophagy accompanied by inhibited growth, photosynthesis, and induced accumulation of ROS. This study provides a basic framework to select key pathways to target in the development of building plant resilience towards non-canonical salt stress induced by excess K^+.

Keywords

K-induced salt stress, potassium transport, transcriptomics, metabolomics, ionomics, molecular phenotype, abiotic stress, nitrogen metabolism, osmoprotectants, antioxidants, antagonistic pleiotropy

Introduction

Can excess potassium (K) in soil be too much of a good thing for plants? Its role as an essential macronutrient for plants is well established and K constitutes 2-10% of plant dry weight (Wang and Wu, 2013). The cytosolic concentration of K^+ is around 100 mM and the vacuolar concentrations generally range between 20-200 mM depending on tissue, developmental age, or species (Leigh and Wyn Jones, 1984; Ashley et al., 2006). These concentrations are typically higher than soil concentrations found in most agricultural soils (Maathuis, 2009) and therefore the vast majority of studies have only investigated uptake into plants from low K^+ concentrations in the soil. As a result, we hardly know if excess K^+ in soils would be as toxic as high Na^+ (Pantha and Dassanayake, 2020), and if it is, how it exerts plant toxicity effects that may be different from Na-induced salt stress seen for high salt concentrations known to cause plant toxicity (>100 mM NaCl). While toxicity on plants at high concentration of other nutrients, such as boron (Aquea et al., 2012; Wang et al., 2021), copper (Lequeux et al., 2010), and nitrogen (Yoshitake et al., 2021), have been investigated, the molecular mechanisms behind K^+ toxicity responses are virtually unknown.

The need to use alternative agricultural lands and recycled wastewater amidst diminishing freshwater resources is intense (IPCC, 2019). These needs cannot be addressed without foundational knowledge on how plant nutrient balance is achieved when conventional land use and irrigation practices no longer provide adequate solutions. Within the US as well as around the world, there are many regions that are naturally high in K^+ content in the soil (Duval et al., 2005). Many industrial as well as agricultural processing plants produce wastewater with exceptionally high K^+ concentrations considered excess for plant growth (Arienzo et al., 2009). During wastewater treatments, unlike N, P, or organic matter which are typically processed using microbial activity, K is concentrated due to evaporation (Arienzo et al., 2009). Therefore, knowing the tolerance mechanisms against high K, which can cause osmotic stress similar to Na on top of additional stresses because of its role as a major nutrient in plants, are imperative toward designing robust crops in our quest to convert marginal lands into productive agricultural lands and reclaim land left unusable due to irrigation practices such as the use of recycled wastewater.

How high K^+ in soils affect plant growth is not a new question for plant scientists (Eijk, 1939). Past studies have reported that high concentrations of K^+ severely affected growth and other developmental processes when tested in a handful of species. For example, growth of *Salicornia herbacea* was induced by 166, 250, and 333 mM NaCl but reduced when treated with the same concentrations of KCl, implying ion specific detrimental effects of K^+ in a halophyte known to be able to cope with high salinity stress (Eijk, 1939). Additional studies using other halophytes including, *Suaeda aegyptiaca* (Eshel, 1985), *S. salsa* (Wang et al., 2001), and several *Atriplex spp.* (Ashby and Beadle, 1957; Matoh et al., 1986; Ramos et al., 2004) have shown that KCl is more toxic than NaCl at similar osmotic strengths. Recently, Richter et al., (2019) compared the effects of 100 mM NaCl, 50 mM Na_2SO_4, and 100 mM KCl and reported that K^+ caused greater physiological and metabolic responses compared to Na^+ in *Vicia faba*. These studies suggest that K^+ may not elicit the same physiological, metabolic, or genetic responses Na^+ does and plants may require distinct genetic pathways in addition to canonical salt response pathways to survive high K-induced salt stress.

In this study, we aimed to identify K-induced salt stress responses and deduce the underlying cellular mechanisms plants have evolved to adapt to K^+ toxicity. We compared *Arabidopsis thaliana* (Col-0 ecotype), a model sensitive to high K^+, to its extremophyte relative, *Schrenkiella parvula* (Lake Tuz ecotype) that thrives in high K^+ soils (Nilhan et al., 2008; Oh et al., 2014). We examined multi-omics level features and responses exhibited by the two model species to high K^+ treatments to identify the relevant genetic pathways influential in regulating or are affected by K^+ toxicity responses. Our results revealed an extensive ionomic, metabolic, and transcriptomic reprogramming during high potassium stress in the stress-sensitive model while providing novel insights into how a stress-adapted model had evolved cellular mechanisms to tolerate K^+ toxicity via metabolic and transcriptomic adjustments.

Materials and methods

Plant material, growth conditions, and stress treatments

Plants were grown at 125-150 µmol $m^{-2}s^{-1}$ photon flux density at a photoperiod of 12 h light, 12 h dark, 23°C, and 60% relative humidity for all the experiments unless it is mentioned

otherwise. For transcriptome, ionome, and metabolome profiling, *Arabidopsis thaliana* (Col-0) and *Schrenkiella parvula* (Lake Tuz ecotype) plants were grown hydroponically in 1/5th strength Hoagland's solution as described in Wang et al., 2021. 25-day-old seedlings (days after germination) were transferred to fresh hydroponic growth media at control conditions or supplemented with 150 mM KCl. Samples were harvested at 0, 3, 24, and 72 hours after treatment (HAT) as summarized in Fig S1. Shoot and root tissue samples were harvested on a randomized basis from the same growth chamber, at the same time of day for control and salt-treated plants. Roots were briefly dried with a paper towel to soak any excess growth solution. At least five plants per sample were harvested in at least three biological replicates (Fig S1). All treatment and harvest times were set at 4 h after the beginning of the light cycle to avoid variation due to circadian effects. The salt treatment was non-lethal based on our preliminary tests using a series of salt concentrations.

The primary root length, lateral root number and density, and root hair length were quantified using plate-grown seedlings. For this, surface-sterilized seeds were germinated in Petri plates on 1/4th Murashige and Skoog (MS) medium (Murashige and Skoog, 1962) solidified with 0.8% Phyto agar (PlantMedium) and grown for 5 days. The seedlings were transferred to 13 cm-diameter large Petri plates with the same media supplemented with different concentration of salts and further incubated in a vertical position to allow better root growth. All measurements were completed before the primary root reached the bottom of the plates. Microscopic images of root hairs were obtained using a Zeiss Lumar brightfield microscope with a 1.5 X FWD 30 mm objective. Plants were imaged for lengths of roots, root hair, and leaf area measurements and quantified using ImageJ (Ferreira and Rasband, 2012). Lateral root density was calculated by dividing the total number of lateral roots with the total length of the primary root in centimeters.

For the plants grown in soil, seeds were directly germinated in 5.5"x5.5''x2.5" pots with SunGro MetroMix 360 soil (SunGro Horticulture, Agawam, MA). The plants were watered with 1/5th strength Hoagland's solution once every week and with tap water every other day. 21 days-old *A. thaliana* and *S. parvula* plants were watered with tap water or 50-400 mM NaCl or KCl salt solutions for control and salt treated plants, respectively, every other day for 14 days.

CO_2 assimilation rates

CO_2 assimilation rates were measured on hydroponically grown plants using a LiCor 6400XT portable system attached to a 6400-17 whole plant Arabidopsis chamber mounted with a 6400-18 RGB light source (LiCor Inc, Lincoln Nebraska). Rates were measured on 25-day old *A. thaliana* and *S. parvula* plants at 0, 3, 24, and 72 h after exposure to 150 mM KCl. Individual plants were placed in a 15 ml centrifuge tube containing the appropriate treatment solution and the centrifuge tube was inserted into a sealed 38 mm Cone-tainer™ mounted in the whole plant Arabidopsis chamber. The chamber was kept at a slight positive pressure and CO_2 exchange was minimal for centrifuge tubes containing nutrient solution with no plants. CO_2 assimilation rates were measured at 400 µL L^{-1} CO_2, 1,000 µmol photons m^{-2} s^{-1}, a chamber temperature of 23°C and an air flow rate of 500 mL min^{-1} after CO_2 assimilation rates were constant (usually within 5 minutes for *A. thaliana* and 10 minutes for *S. parvula*). Measurements were made on 3 replicate plants.

Ionome and Total C and N profiling

For each time point and condition described in Fig S1, four biological replicates were harvested and dried for 1 week at 40°C and weighed daily until the dry weights stabilized before grinding. The sample preparation for ionome measurements was performed following Ziegler et al. (2013). Briefly, 10-30 mg of dried samples were digested with 2.5 mL concentrated HNO_3 (AR Select Grade, VWR International, LLC) at room temperature overnight and heated at 105°C for 2 h. Each sample was diluted to 10 mL with ultrapure 18MΩ water (UPW) and 0.9 mL of the diluted extract was further mixed with 4.1 mL UPW to a 5 mL final volume, of which 1.2 mL was used for ICP-MS (inductively coupled plasma mass spectrometry). Concentrations of 21 elements (K, P, Mg, S, Ca, Al, Zn, Co, Ni, Fe, Se, Cu, B, Mn, Mo, As, Rb, Cd, Na, Li, and Sr) were quantified at USDA-ARS-Plant Genetics Facility, Donald Danforth Plant Science Center, as described in Baxter et al. (2014), using a Perkin Elmer NexION ICP-MS platform with 20 µg L^{-1} In as an internal standard (Aristar Plus, BDH Chemicals). Results were visualized as heatmaps using the 'pheatmap' R package (v. 1.0.12) (Kolde, 2012). Total carbon and nitrogen were quantified using a Costech 4010 elemental analyzer (Costech, Valencia, CA, US). Each sample ranged from 2-10 mg ground tissue. Acetanilide and 4 mg of wheat flour were used as internal controls.

One-way ANOVA, followed by Tukey's post hoc test ($p<0.05$) was performed using the agricolae R package for 3-4 biological replicates to determine significant changes.

Metabolite profiling

To obtain high-throughput metabolite profiles on samples described in Fig S1, we performed non-targeted gas chromatography-mass spectrometry (GC-MS) at the Fiehn Laboratory, West-coast Metabolomics Center at UC-Davis. Following harvest, both root and shoot samples were immediately frozen in liquid nitrogen and processed as described in Fiehn et al. (2008). A Leco Pegasus IV mass spectrometer with the following parameters were used: unit mass resolution at 17 spectra per second with a scan mass range of 85-500 Da at 70 V ionization energy and 1800 V detector voltage with a 230°C transfer line and a 250°C ion source. Raw data files were processed using ChromaTOF vs. 2.32 with automatic mass spectral deconvolution followed by peak detection at 5:1 signal/noise levels for all chromatograms. The BinBase database was used for automated annotation of detected peaks to metabolites (https://bitbucket.org/fiehnlab/binbase/src/master/). To generate relative abundance values, we used peak heights of specific retention indices which allows greater separation between metabolites and higher detection capacity for less abundant metabolites. The raw abundance/intensity for each identified compound was normalized with a series of fatty acid methyl esters (xylulose, oleamide, mannonic acid, enolpyruvate, dihydroxymalonic acid, coniferin, butyrolactam, 2-ketoglucose dimethylacetal, and 2,5-dihydroxypyrazine) used as National Institute of Standards and Technology (NIST) internal standards. Significance tests were performed using one-way ANOVA followed by Tukey's post hoc test at $p<0.05$ in the agricolae R package for at least three biological replicates and circular plots to visualize selected metabolites were generated using the circlize package in R (Gu et al., 2014).

RNA-seq analyses

Total RNA from three biological replicates of root and shoot tissues harvested at 0, 3, 24, and 72 h after treating with 150 mM KCl (Fig S1) were extracted (~6 µg) using RNeasy Plant Mini Kit (Qiagen, Hilden, Germany) with column digestion to remove DNA contamination. Six to eight plants were pooled for each replicate. A total of 48 RNA-seq libraries were prepared using the TruSeq RNA library preparation kit (Illumina, San Diego, USA) and sequenced on an Illumina

HISeq 4000 platform at the Roy J. Carver Biotechnology Center, University of Illinois at Urbana-Champaign. A total of 12-23 million 50-bp reads was obtained from each library (available at NCBI-SRA database under BioProject PRJNA63667). Following quality checks using FastQC (Andrews, 2010), RNA-seq reads uniquely mapped to *A. thaliana* TAIR10 or *S. parvula* (Dassanayake et al., 2011) v2.2 gene models (https://phytozome-next.jgi.doe.gov/), were quantified using Bowtie (Langmead et al., 2009) and a custom script as described in (Pantha et al., 2021).

Differentially expressed genes (DEGs) between K^+ treated and control samples were identified using DESeq2 with an adjusted p-value cutoff 0.01 (Love et al., 2014). DEGs shared between treatments were plotted using UpSetR (Conway et al., 2017). Orthologous gene pairs between the two species were identified using the CLfinder-OrthNet pipeline with default settings (Oh and Dassanayake, 2019) and further refined as described in Wang et al. (2021) to include lineage-specific genes and duplications. For ortholog expression comparisons between *S. parvula* and *A. thaliana*, regularized log (rlog) values estimated by DESeq2 were normalized per each gene. Ortholog pairs compared to the median across all samples were used to determine temporal co-expression clusters based on fuzzy k-means clustering (Gasch and Eisen, 2002) with a membership cutoff set to 0.5. From initially identified 10 root and 11 shoot clusters (Table S11), we filtered out clusters that did not show a response to K treatments in both species and identified 5 root and 3 shoot co-expression super clusters with distinct response trends. All expressed genes were assigned Gene Ontology (GO) annotations when available and DEGs with GO annotations were used to identify enrichment processes using BinGO (Maere et al., 2005). To summarize functional groups enriched among DEGs, redundant GO terms with > 50% overlap were further clustered using GOMCL (Wang et al., 2020). DEGs were also annotated based on KEGG pathways (Kanehisa et al., 2016). Functional processes identified with specific GO terms which included more than 20 but no more than 500 DEGs to represent a function were used for functional enrichment analysis monitored temporally in roots and shoots. This avoided inclusion of functions represented by a few genes and any process that had large number of genes that resulted in broad or generic descriptions from the

comparison. Heatmaps for gene expression visualization were generated using the 'pheatmap' R package (v. 1.0.12) (Kolde, 2012).

Histochemical detection of hydrogen peroxide and superoxide

Histochemical detection of H_2O_2 was performed on 25 days-old hydroponically grown *A. thaliana* and *S. parvula* plants using 3,3'-diaminobenzidine (DAB, Sigma-Aldrich, Poland) which is oxidized in the presence of H_2O_2 and forms a brown stain (Daudi and O'Brien, 2012). We further assessed the formation of superoxide during high K^+ stress using nitroblue tetrazolium (NBT) (Thermo Fisher Scientific) which in the presence of O_2^- forms a purple stain (Jabs et al., 1996). The DAB and NBT solutions were applied on leaves under a gentle vacuum infiltration for 5 minutes followed by shaking at 100 rpm for 4 h. Five mL of 10 mM Na_2HPO_4 without staining solutions was used as a negative control. Staining solutions were replaced with a bleaching solution (ethanol: acetic acid: glycerol = 3:1:1) for destaining chlorophyll by boiling for 15 minutes. Destained leaves were imaged using a Zeiss Lumar microscope with x0.8 magnification. We tested three plants per condition and two leaves per plant.

Results

KCl is more toxic than NaCl at the same osmotic strengths

High K^+ is different from Na^+ in how it affects plant growth (Fig 1A-E). Independent of plant age (Fig 1A,B) and tissue type (Fig 1C,E), K^+ exerts severe growth disturbances than observed for Na^+ at the same concentrations in both species. For example, *A. thaliana* treated with 100 mM KCl did not survive more than a week after completion of treatment to complete its reproductive cycle, while 100 mM NaCl treated plants could complete their life cycle despite the apparent adverse effect on growth (Fig 1B). It should be noted that the growth media used in the current study included 1.2 mM K^+ to support plant growth in all conditions and the ≥50 mM KCl treatments provide excess K^+ beyond its expected range serving as a nutrient (0.1-6 mM) (Ashley et al., 2006). The more tolerant species, *S. parvula*, required higher concentrations of KCl than *A. thaliana* before it showed significant defects in both primary and lateral growth (Fig 1C). *S. parvula* root hair length was also less affected compared to that in *A. thaliana* (Fig 1D, S2). Compared to the same concentration of NaCl treatments, KCl seemed to be more toxic

even to the more salt stress-tolerant *S. parvula* (Fig 1A-E). These results suggest that despite similar levels of osmotic stress elicited by K^+ and Na^+ at equal concentrations, K^+ may exert additional stresses different from Na^+ that may initiate physiological responses specific to K^+ stress.

Because plant growth is tightly coupled to photosynthesis, we tested how the rate of CO_2 assimilation was affected by K^+ toxicity. CO_2 assimilation was reduced in *A. thaliana* in response to 150 mM KCl within 24 hours after treatment (HAT), but *S. parvula* did not show any short-term effects (Fig 1F) even when there was a significant reduction in total leaf area in both species under longer-term treatments (Fig 1E). Consequently, in *A. thaliana*, the total carbon content in shoots declined within 72 HAT (Fig 1G).

Overall, 150 mM KCl was sufficient to induce physiological stress phenotypes in roots and shoots of *A. thaliana* within a 3-day period, while impacting long-term growth in *S. parvula* (Fig 1). Notably, 150 mM KCl treatment given for more than a week was lethal to *A. thaliana* in all tested growth conditions. Therefore, we selected 150 mM KCl for our cross-species comparative-omics analyses to investigate K^+ toxicity responses, when both species are expected to show active cellular responses to minimize or tolerate stress during the early stages of the treatment at 0, 3, 24, and 72 HAT (Fig S1).

Excess K^+ causes nutrient depletions in *A. thaliana* but not in *S. parvula*

Given the role of K as an essential macronutrient, plants have evolved multiple transporters to facilitate entry of K^+ into roots rather than its exit pathways (Shabala and Cuin, 2008). Therefore, we first hypothesized that high K^+ in soils will lead to high K^+ contents in plants and shoots will accumulate more of the excess K^+ in the transport sequence from soil-root-shoot. Second, we predict that the differential accumulation of K^+ in roots and shoots will alter many cellular processes and thereby affect transport and retention of other nutrients. To test our hypotheses, we quantified the root and shoot contents of 16 established plant nutrients (K, N, P, Mg, S, Ca, Al, Zn, Co, Ni, Fe, Se, Cu, B, Mn, and Mo) and six toxic elements found in most soils at low concentrations (Fig 2) in hydroponically grown *A. thaliana* and *S. parvula*. Nitrogen was measured separately but from the same plant samples (see methods and Fig S1). With ionomic profiling, we aimed to test if (a) K^+ would accumulate in plants as an

isolated process decoupled from other element accumulation; (b) high K^+ treatment would cause nutrient imbalances; or (c) it allowed entry of other toxic elements and could indirectly cause toxicity symptoms.

We observed three notable trends in how the two species partitioned K between roots and shoots (Fig 2A). First, both species kept higher K^+ levels in shoots than in roots, but the difference between shoots and roots was strikingly larger in *S. parvula* than in *A. thaliana,* under control conditions (*i.e.* 0 HAT before exposure to excess K^+). Second, *A. thaliana* reduced the root K^+ levels by 24 HAT compared to 0 HAT, but was unable to maintain the lower K^+ level with prolonged stress, leading to significantly increased K^+ levels in both roots and shoots by 72 HAT. Third, *S. parvula* maintained a significantly lower K^+ content in the roots compared to *A. thaliana* throughout the stress treatment even when the root K^+ levels increased over time compared to the control. Importantly, *S. parvula* was able to maintain shoot K^+ levels comparable to the control (Fig 2A). While both species had a higher total K^+ content in shoots than in roots, only *A. thaliana* allowed a further increase in its shoot K^+ content under the current experimental conditions. *S. parvula* appeared to avoid using shoots as a sink for excess K^+ compared to *A. thaliana*.

Higher accumulation of K^+ in *A. thaliana* was not an isolated process and it was coupled to a severe nutrient imbalance leading to the depletion of seven nutrients (Fig 2B-D). In line with uninterrupted root growth observed under high K^+ stress (Fig 1A), *S. parvula* did not show a nutrient imbalance. As summarized in Figures 2D and 2E, *S. parvula* showed a remarkable capacity in maintaining major macronutrients (C, N, and P) at steady states upon exposure to excess K^+, while in *A. thaliana* all three major nutrients were depleted as K^+ significantly accumulated over time in both roots and shoots.

We further observed that excess K^+ did not cause accumulation of any other element that could cause indirect toxicity effects in either species (Fig 2C). Therefore, we can rule out the possibility of observing indirect toxicity effects from other non-nutrients in downstream analyses to deduce cellular processes affected by excess K^+. Depletion of Na in roots (Fig 2C) in both species indirectly showed the effort by both species to limit the entry of K^+ and/or increase export using K/Na transporters or channels that can act non-selectively on both ions.

However, the overall effects on the ionomic profiles indicated that a greater capacity to extrude K^+ from the soil-root interface or prevent entry into the roots from soil cannot be the only major mechanism underlying K^+ toxicity tolerance in *S. parvula*. For example, *S. parvula* showed higher fold-increase of root K upon KCl treatment although the overall K content was still lower than the K content in *A. thaliana* roots (Fig 2A).

S. parvula is more responsive than *A. thaliana* at the metabolome level to high K^+ stress

We obtained 472 metabolites of which 145 is known and 327 were unannotated (Table S1) to expand our search to identify cellular processes influencing responses to high K^+ stress (Fig 3). Interestingly, we found that *S. parvula* roots, which showed minimal changes at the physiological and ionomic levels compared to *A. thaliana* during high K^+ stress, was more responsive at the metabolomic level (Fig 3A). Considering the higher fraction of unannotated and hence unknown metabolites in metabolite profiles (Table S1), we tested if the unknown metabolite pool had a similar response trend to the known metabolites identified between the two species (Fig 3B). In all tissue/time points, we observed a high correlation of relative abundances of metabolites, whether known metabolites (Fig 3B, r) or all metabolites including unknowns (Fig 3B r') were considered. For downstream analysis, we only considered the known metabolites with significant abundance changes (abbreviated as MACs for this study) between control and KCl treated conditions (Fig 3A). We further categorized them into (1) amino acids and immediate precursors or derivatives, (2) fatty acids and lipids, (3) nucleic acids, (4) organic acids and their immediate derivatives, and (5) sugars, sugar alcohols, and their associated derivatives (Table S1, Fig 3C).

Overall, the metabolic profile comparisons between the two species showed three distinct trends. First, with longer stress durations, the number of MACs increased in all tissues for both species (Fig 3A,C). Second, shoots had more MACs in *A. thaliana*, while *S. parvula* contained more MACs in roots in response to excess K^+ (Fig 3A,C). The higher responsiveness of the shoot metabolome in *A. thaliana* is aligned with our initial hypothesis that we would expect more metabolic disturbances in photosynthetic tissues when excess K^+ accumulated more in shoots (Fig 2A). Contrastingly, the *S. parvula* root metabolome was more responsive compared to both the metabolomes of *A. thaliana* root and *S. parvula* shoot (Fig 3C), suggesting an

alternative response strategy of adjusting predominantly the root metabolites in a species more tolerant to K^+ toxicity. Third, increased abundances of multiple primary metabolite pools especially in *S. parvula* roots (Fig 3D, Root, outer circle) were conspicuous against the overall depletion of primary metabolites in *A. thaliana* in all tissues/time points (Fig 3D, Root and Shoot, middle circle). One of the largest groups that changed in metabolite abundance during high K^+ stress was amino acids and their derivatives in *S. parvula*. Further, sugars and the associated metabolite pools changed highly in roots of both species and also in *A. thaliana* shoots. This suggested that the two species primarily used different metabolic groups/pathways to respond to high K^+ stress, a notion further supported by few cross-species overlaps among MACs (Fig 3A). Therefore, we further examined how amino acids and sugars significantly changed from control to high K^+ stress conditions over time.

Species specific MACs can indicate metabolic pathways or metabolite groups that are responding to minimize cellular toxicity, severely interrupted by stress, or both. Excess K detrimentally affected *A. thaliana* but hardly interrupted the growth of *S. parvula* (Fig 1). Therefore, we explored the possibility that metabolic pathways or groups represented by MACs in *S. parvula* were enriched in pathways acting towards minimizing cellular stress, while MACs in *A. thaliana* were more representative of pathways or groups disrupted by high K^+ stress. More sugars and amino acids that can serve as osmolytes (raffinose, myo-inositol, sucrose, and proline) (Fig 3D) (Gong et al., 2005) during salt stress increased in *S. parvula* compared to *A. thaliana.* When we tested for enriched metabolic pathways or metabolite groups among MACs, galactose metabolism was enriched in *A. thaliana* shoots and *S. parvula* roots (Fig S3A). The metabolites in galactose metabolism (KEGG Pathway ID:ath00052) included several key metabolites (for e.g. galactinol, myo-inositol, and raffinose) (Fig S3B) which are known to protect plants against oxidative and osmotic stresses (Taji et al., 2002; Nishizawa et al., 2008). Interestingly, these increased uniquely in *S. parvula* roots (Fig S3B), suggesting coordinated metabolic adjustments balancing C and N sources to maintain growth while minimizing damage from oxidative bursts in *S. parvula* roots. Overall, the more stress tolerant species seemed to boost the protective metabolite pools while the more stress sensitive species was depleting its initial pools for such protective metabolites during stress.

A. thaliana shows wide-ranging misregulation of transcriptional resources during peak stress response times reflective of its critical failures to maintain cellular processes

We next examined the transcriptional stress response landscapes and sought to deduce specific cellular processes initiated by *A. thaliana* and *S. parvula* after exposure to high external K^+. Such cellular processes could further build on time-dependent physiological, ionomic, and metabolic processes we identified earlier in this study as responses to excess K^+ accumulation. We obtained 12-23 million reads per RNA-Seq library prepared from three biological replicates of root and shoot samples of both species, harvested at four time points (0, 3, 24, and 72 HAT) (Fig S1). A total of ~70 - 90% reads were uniquely mapped to primary protein-coding gene models in *A. thaliana* (TAIR10) and *S. parvula* (V2.2) reference genomes (Table S2).

The Principal Component Analysis (PCA) on shoot and root transcriptomes clustered samples based on the treatment time points with *A. thaliana* showing a greater separation between conditions compared to *S. parvula* (Fig S4A). The individual transcriptomes in pairwise comparisons showed a higher correlation within *S. parvula* samples than for *A. thaliana* samples (Fig S4B). Overall, *S. parvula* had fewer transcriptome-wide changes in response to high K^+ stress than *A. thaliana.* PCA on 23,281 ortholog pairs identified between the two species further supported that *A. thaliana* transcriptomes had a greater variance along a temporal trajectory for duration of exposure to excess K^+, while *S. parvula* showed a similar trajectory but with a much smaller variance (Fig 4A). The total number of differentially expressed genes (DEGs) that showed a significant response in at least one time point was remarkably higher in *A. thaliana* (9907 in roots and 12574 in shoots) compared to that in *S. parvula* (1377 in roots and 494 in shoots) (Fig S5 and Table S3). This observation led us to question whether the stress sensitive *A. thaliana* is transcriptionally adjusting and concurrently failing to maintain steady levels of critical cellular processes, while the more stress tolerant *S. parvula* is only responding with minimal adjustments to a subset of processes *A. thaliana* may be adjusting suboptimally. Therefore, we first identified the key cellular processes and pathways *A. thaliana* was transcriptionally adjusting, to deduce processes interrupted or misregulated due to excess K^+ as well as processes likely activated for protective roles.

We annotated all DEGs with a representative Gene Ontology (GO) function (Table S4, S5, S6) and examined their time dependent progression in *A*. *thaliana* (Fig 4B and S5). The temporal transcriptomic response climaxed at 24 HAT as shown by having the highest number of DEGs and the largest number of enriched cellular functions. Additionally, the shoots lagged behind the root responses (Fig 4B). This lag is reflected by the most number of DEGs and enriched functions observed during 3-24 HAT in roots and 24-72 HAT in shoots. Despite the response time lag, the enriched processes are largely shared between roots and shoots in *A. thaliana* (Fig 4B).

One of the most emergent cellular process categories enriched in both roots and shoots in *A. thaliana* was response to stress (Fig 4B). Within this category, the prevalent specific responses across all time points were responses to salt, oxidative, and ionic stresses. Unexpectedly, biotic stress-related GO terms (e.g. response to bacterium, response to chitin, and immune response) were also prominently enriched at all time points (Fig 4B). Induction of biotic stress responses in *A. thaliana* seemed counterintuitive when the *S. parvula* orthologs of these *A. thaliana* high K^+-induced DEGs were mostly suppressed in response to high K^+ stress (Table S3 and S7). Given that *A. thaliana* shows a peak transcriptional response at 24 HAT, this made us question whether we were observing transcriptional chaos rather than targeted transcriptional resource allocation between biotic and abiotic stresses to manage the extant stress experienced by *A. thaliana*.

We observe three indicators to suggest that there is overall misregulation in critical signaling pathways that highlight chaotic and inefficient responses to overcome cellular toxicity intensified due to excess K^+ accumulation in *A. thaliana* (Fig 2). First, the cellular response to stress in shoots included enriched functions representing all major plant hormone pathways (Fig 4B). In addition to the ABA response enriched at all time points, all other major plant hormone responses are elicited concurrently during 24-72 HAT in shoots in the absence of canonical developmental or biotic stress cues, suggesting disruptions in hormone signaling. Second, we find autophagy as the most enriched process with the highest proportion of DEGs (24 DEGs or 60% of all annotated, adjusted p-value 9.39E-07), accompanied by additional processes including cell death and leaf senescence, enriched during 24-72 HAT in shoots. Third,

we see enriched responses to cold, heat, wounding, drought, and hypoxia which all share common genetic mechanisms with responses to oxidative stress also prevalent during 24-72 HAT (Fig 4B). This suggested unmitigated oxidative stresses. We compared the ROS scavenging capacity between *A. thaliana* and *S. parvula* leaves during high K^+ stress, by assessing the accumulation of oxidative stress markers, H_2O_2 and O_2^-. As predicted by the transcriptional response, leaves of *A. thaliana* showed greater levels of oxidative stress compared to *S. parvula* (Fig 4C). While the reduced numbers of DEGs at 72 HAT especially in roots indicated a degree of acclimation in *A. thaliana* (Fig. 4B and S5B), the prolonged ABA signaling together with non-specific activation of hormone pathways, autophagy, and oxidative stresses serve as molecular phenotypes that indicate erratic and inefficient responses especially in *A. thaliana* shoot, which could lead to eventual failures in cellular homeostasis after prolonged exposure to high K^+ stress as supported by the observed growth phenotypes (Fig 1). These molecular phenotypes become even more compelling when compared to their respective transcriptional profiles in *S. parvula* orthologs which remained mostly unchanged (Fig 4D).

Primary metabolic processes involving carboxylic acid/carbohydrate and amino acid metabolism form the second largest group among the most affected transcriptional categories (following stress responses), found to be enriched in all time points during high K^+ stress in both *A. thaliana* roots and shoots (Fig 4B). This further supports the previous physiological and metabolic responses that showed primary C and N metabolism pathways were severely affected (Fig 1F and G, Fig 3C and D). Notably, most transcriptional adjustments to C and N metabolism were detected at later time points. For example, interruptions to photosynthesis at 24 and 72 HAT (Fig 1F) were aligned with the corresponding transcriptional processes enriched at the same time points in *A. thaliana* shoots (Fig 4B). On the contrary, growth responses influenced by nutrient homeostasis during stress, such as root development, was detected as a transcriptionally enriched process early at 3 HAT (Fig 4B), although the interruptions to root hair growth was detected later at 72 HAT (Fig 1D).

S. parvula shows a confined yet a targeted transcriptomic response steered towards stress tolerance while supporting enhanced C-N metabolism

We searched for DEGs among *A. thaliana* whose *S. parvula* orthologs also showed active responses (Fig 5A). These ortholog pairs likely represent cellular processes that require active transcriptional adjustments to survive the accumulation of excess K^+ in plant tissues even in a more stress tolerant species. We predicted that the transcriptional adjustments in diametric responses between the species will be detrimental to the stress sensitive species, while shared responses in similar directions will be beneficial yet likely underdeveloped or unsustainable to survive the stress by the stress sensitive species. There were fewer ortholog pairs showing diametric responses (256 and 60 ortholog pairs in roots and shoots, respectively) compared to those with shared responses (305 and 283 in roots and shoots respectively) between *A. thaliana* and *S. parvula* (Fig 5A, S5).

Among the diametric responses, the largest functional cluster identified as induced in *A. thaliana*, while suppressed in *S. parvula* roots was response to stress (Fig S5A). Most of the subprocesses in this cluster are associated with biotic stress (Table S9). Therefore, we further assessed this transcriptional divergence between the two species as a proportional effort invested in biotic vs abiotic stress responses out of the total DEGs responded in at least one time point within each species (Fig 5B). The effort to suppress biotic stress responses in *S. parvula* roots (10%) was similar to the proportional induction for biotic stress responses in *A. thaliana* (9%) within total non-redundant DEGs (Fig 5B). Contrarily, orthologs that were suppressed in *A. thaliana*, but induced in *S. parvula* roots were associated with ion transport and cell wall organization (Fig S5A). These transcriptional adjustments support the physiological response in *S. parvula* where new roots grew uninterrupted maintaining ion uptake during exposure to excess K^+, compared to *A. thaliana* roots that failed to keep nutrient uptake and subsequently stopped growing (Fig 1C and 2C). In shoots, orthologs induced in *A. thaliana* but suppressed in *S. parvula* include multiple genes associated with defense responses, corroborating our observation of the erratic transcriptional resource allocation to biotic stress responses in *A. thaliana* (Fig S5B). The orthologs suppressed in *A. thaliana* but induced in *S. parvula* shoots were enriched in carboxylic acid and amine metabolism and associated transport functions (Fig S5B). This reflects the transcriptional undertaking in *S. parvula* that supports continued growth (Fig 1B,C,E,F), upheld nutrient balance (Fig 2B,C,D,E), and induction

of metabolite pools associated with C and N metabolism (Fig 3C,D) during high K^+ stress, while *A. thaliana* shows opposite physiological, ionomic, and metabolic responses.

The ortholog pairs that showed shared induction (156 and 199 in root and shoot, respectively) in *A. thaliana* and *S. parvula* were largely represented by abiotic stress responses mediated by hormones including ABA (Fig S5 and Table S10). The ortholog pairs with shared suppression (149 and 84 in root and shoot, respectively) were enriched in functional processes involved in biotic stress in roots and photosynthesis in shoots. Therefore, at least in roots, *A. thaliana* seems to actively reduce its transcriptional allocation to biotic stress via subsets of genes regulated congruently with *S. parvula* (Fig S5A). However, genes showing this pattern were negligible based on a proportional effort (0.004% in *A. thaliana*) to reduce transcriptional allocation to biotic stress responses compared to *S. parvula* (10%) in roots (Fig 5B).

Over 50% of orthologs differently expressed in response to excess K^+ in *S. parvula* roots and ~30% in shoots show unique expression trends different from *A. thaliana* (Fig 5A). Both *S. parvula* specific responses and diametric responses between the two species were more pronounced in roots than in shoots. We predicted that *S. parvula* activates decisive transcriptional regulatory circuits that are either absent (*i.e. S. parvula*-specific responses) or wired differently (*i.e.* diametric responses) in roots than in shoots when responding to excess K^+ stress.

The overall transcriptomic response of *S. parvula* encapsulates induction of more targeted salt stress responses compared to *A. thaliana*, including especially oxidative stress responses, sugar and amino acid metabolism, and associated ion transport, with concordant induction in growth promoting processes and transcriptional resource recuperation by suppressing biotic stress responses (Fig 5C). The transcriptional effort to facilitate growth amidst excess K^+ accumulation in tissues is reflected by induced transcripts involved in cell wall biogenesis, RNA processing, and development along with concurrent suppression for rapid growth limiting processes such as cell wall thickening and callose deposition (Table S10).

Differential expression of K^+ transporters lead to differential compartmentalization of excess K^+ concurrent to extensive stress signaling cascades triggered in *A. thaliana*

Our ionome profile comparisons demonstrated that *A. thaliana* exposed to high external K^+ over time accumulate K^+ in its tissue concurrently with the depletion of C, N, and P at a whole plant level (Fig 2). Additionally, transcriptional responses to excess K^+ had ion transport among the most represented functions within and between species comparisons (Fig 4B, 5C, and S5A). The ability in *S. parvula* to curb K^+ accumulation and prevent the depletion of major nutrients led us to hypothesize that K^+ transporters are differentially expressed in the two species as a first line of defense against a severe nutrient imbalance during excess K^+ stress. Among over 70 transporters reported to transport K^+ in *A. thaliana* (Shabala and Cuin, 2008), we predicted that the transcripts coding for K^+ transporters which allow K^+ into roots and upload K^+ into the xylem or phloem would be primary targets for down-regulation in the effort to restrain K^+ accumulation. On the other hand, transcripts sequestering K^+ into the vacuoles, especially when tissue [K^+] is high, will be induced. To assess these predictions, we checked the transcript profiles of all known K^+ transporters.

We first searched for K^+ transporter transcripts that showed significantly different basal level abundances (Fig 6A) and responses to high K^+ stress (Fig 6B) between *A. thaliana* and *S. parvula*. We categorized four transport routes that would limit accumulation of K^+ in plants and compartmentalize excess K^+ within tissues or cells: a. limit entry into roots, b. promote efflux from roots, c. constrain long distance transport between root and shoot, and d. enhance sequestration into vacuoles. We then sought to find out routes that are potentially failing to keep up with the mounting stress in *A. thaliana* and/or more strategically exploited by *S. parvula*.

a. Limit entry into roots. The most suppressed gene in *A. thaliana* under excess K^+ stress is the *high-affinity K^+ transporter 5* (*HAK5*) that showed a 13-fold reduction at 24 and 72 HAT. At low soil K^+ levels, the major transporter for K^+ uptake in roots is HAK5. This mode of K^+ transport switches to low affinity transport mediated by the K channel AKT1 that requires the channel subunit KC1 to function at sufficient K^+ levels in soil (Gierth et al., 2005; Xu et al., 2006; Wang et al., 2016) These two major transporters are activated post-translationally by the protein kinase complex calcineurin B-like proteins 1 and 9 (CBL1&9)/CBL-interacting protein kinase 23 (CIPK23) (Ragel et al., 2015). Under excess K^+ stress both transport complexes and

their core post-translational regulatory unit in *A. thaliana* roots are suppressed (Fig 6B, C, and S6A). The transcripts coding for the transporters are unchanged in *S. parvula* roots but the interacting partners of the kinase complex are suppressed (Fig 6B and S6A). The transcriptional effort to limit entry of K^+ into roots during high K^+ stress is further exemplified by the suppression of *RAP2.11*, a transcriptional activator of *HAK5* (Kim et al., 2012) and the induction of *ARF2*, a repressor of *HAK5* transcription (Zhao et al., 2016), in *A. thaliana* roots (Fig 6C). Similarly, *ARF2* is also induced in *S. parvula* roots. Other K^+ transporters that are reported to function in K^+ uptake into roots are also suppressed in *A. thaliana* (e.g. KUP6 and KUP8) under excess K^+ stress (Fig 6B). While a similar transcriptional suppression for KUP transporters is absent in *S. parvula* roots, it shows concerted transcriptional suppression of cyclic nucleotide gated channels, *CNGC3/*10/12/13 (Fig 6B and C), suggesting down-regulation of non-selective uptake of monovalent cations including K^+ into roots (Gobert et al., 2006; Guo et al., 2008).

b. Promote efflux from roots. We do not know of any K^+ efflux transporter that functions to extrude excess K^+ from roots back to the soil under excess K^+ conditions. However, *S. parvula,* which has evolved in soils naturally high in K^+, induced transcription of a K^+ outward rectifying channel, *GORK* (Ivashikina et al., 2001) and the Na^+ exporter *SOS1* (Shi et al., 2000) in roots (Fig 6B, C and S7A). Induction of *GORK* is known to cause K^+ leakage from roots under biotic and abiotic stresses in plants leading to programmed cell death (Demidchik et al., 2014). We propose that *S. parvula* has evolved to allow export of excess K^+ via induction of GORK without the destructive downstream consequences of cell death as expected in *A. thaliana* (Fig 6B, C, 4B, and 4D). We also note that the basal expression level of *GORK* in *S. parvula* roots is higher than in *A. thaliana* roots (Fig 6A). Next, SOS1, the antiporter with the highest Na^+ efflux capacity in roots, is known for its Na^+ specificity (Oh et al., 2009). Therefore, induction of *SOS1* in *S. parvula* under high K^+ stress (Fig S7A) is likely an effort to counterbalance the increasing osmotic stress due to elevated K^+ by exporting available Na^+ from roots. This explanation fits with Na^+ being the only ion depleted in *S. parvula* roots during excess K^+ stress (Fig 2C). Similarly, a well-documented Na^+/K^+ transporter family in plants encoded by *HKT1* (Uozumi et al., 2000; Ali et al., 2016) known for its key roles in minimizing Na-induced salt stress, is present as a single copy (AtHKT1) for selective Na^+ transport in *A. thaliana*. In *S. parvula*, among the two

duplicated *HKT1* paralogs, *SpHKT1;2* has been demonstrated to show selective-K^+ transport while Sp*HKT1;1*, orthologous to *A. thaliana HKT1,* shows selective-Na^+ transport (Ali et al., 2018). We observe basal-level expression biases for the *S. parvula HKT1* paralogs, however the K^+-selective paralog, despite its much higher transcript abundance, did not significantly respond to excess K^+ (Fig S7B).

c. Constrain long distance transport between root and shoot. The long-distance transport of K^+ via xylem loading is mediated by SKOR, NRT1.5, and KUP7 in *A. thaliana* (Gaymard et al., 1998; Han et al., 2016; Li et al., 2017). *SKOR* and *NRT1.5* were suppressed in *A. thaliana* roots as predicted. However, *KUP7* showed induction in *A. thaliana* roots at 72 HAT concordantly when K^+ accumulation was observed in shoots following exposure to high K^+ (Fig 6B and 2A). Contrastingly, none of these transporters were differently regulated in *S. parvula* roots. AKT2 is the dominant channel protein regulating long distance transport via loading and unloading to the phloem (Dreyer et al., 2017). It too is significantly suppressed in *A. thaliana* shoots, but unchanged in *S. parvula* roots and shoots (Fig 6B and C).

d. Enhance sequestration into vacuoles. Vacuolar K^+ concentration can fluctuate widely, and this sequestration capacity is tightly controlled with pH of the vacuole primarily regulated by the Na^+,K^+/H^+ antiporters, NHX1 and NHX2. These are spatiotemporally regulated with overlapping functions. Additionally, NHX4 is a more selective K^+/H^+ antiporter functioning to store K^+ in vacuoles at a smaller scale (Bassil et al., 2019). In *A. thaliana* during high K^+ stress, *NHX2* is induced in roots, whereas *NHX1* is induced in shoots. However, the transcriptional signal to promote K^+ sequestration in *A. thaliana* either in roots or shoots is unclear, because in roots *NHX1* is suppressed while in shoots *NHX4* is suppressed (Fig 6B and C). This tissue-specific mixed regulatory pattern observed in *A. thaliana* is absent in *S. parvula*. Nonetheless, *S. parvula* does not show any pronounced transcriptional commitment to enhance transport of excess K^+ into vacuoles in shoots. The nonselective slow-activating vacuolar (SV) channel encoded by *TPC1* (tandem-pore calcium channel) and K^+-selective vacuolar channels (TPK/KCO) play primary roles in regulating the release of K^+ into the cytosol from the vacuole (Voelker et al., 2006; Gobert et al., 2007). Under high K^+ stress, *A. thaliana* induces *KCO6* in roots while keeping *TPC1* unchanged. However, *S. parvula*, through suppression of *KCO5*, seems to attempt to

preferentially retain excess K^+ sequestered in vacuoles in roots (Fig 6B and C). Such an attempt to compartmentalize excess K^+ in vacuoles is further suggested by the suppression of tonoplast localized nonselective cation channels *CNGC19* and *CNGC20* (Yuen and Christopher, 2013) in *S. parvula* roots.

Our initial physiological assessments showed that photosynthesis was decreased at 24 HAT in *A. thaliana* (Fig 1F). The transcriptional signal of K^+ transporters associated with maintaining turgor of guard cells corroborate the physiological observation, by showing a bias towards closed stomata via an induction of *GORK* coordinated with a suppression of guard cell localized *KAT1/2* in *A. thaliana* shoots (Fig 6B and C) (Ivashikina et al., 2001; Szyroki et al., 2001). The comparable regulatory unit for closed stomata is not induced in *S. parvula* shoots as a transcriptomic signal.

Osmotic and oxidative stresses combined in plant tissues entail regulation of water transport mediated by aquaporins and multiple signaling cascades regulated by calcium signaling pathways (Srivastava et al., 2014; Takahashi and Shinozaki, 2019). Accumulation of excess K^+ leads to a sweeping array of differentially regulated aquaporins and calcium signaling pathway genes in both roots and shoots of *A. thaliana* compared to a limited regulation detected for *S. parvula* (Fig S6). This reinforces our overall depiction of the stress response in *S. parvula* to reflect a restrained set of transcriptional responses during excess K^+ stress.

Excess K^+ induced nitrogen starvation and failure to activate key pathways in N-metabolism are critical flaws in *A. thaliana* compared to *S. parvula*

The steep drop in total N content in *A. thaliana* compared to *S. parvula* (Fig 2B and D); reduction in amino acids and derivatives in *A. thaliana* while these metabolites increased in *S. parvula* (Fig 3C and D); followed by suppression of transcriptomic signals associated with amine metabolism in *A. thaliana* when these were induced in *S. parvula* (Fig 4B, 5C, and S5B) necessitated further examination on how excess K^+ may alter N-metabolism in plants. Under low soil K levels, N uptake in the form of nitrate is tightly coupled to K uptake and translocation within the plant. Many of the K and N transporters or their immediate post-transcriptional activators are co-regulated at the transcriptional level (Coskun et al., 2017). We searched for specific transcriptomic cues to determine how N transport was disrupted under high K^+, leading

to a deficiency in physiological processes needed to maintain growth and development or a shortage of protective metabolites against oxidative and osmotic stress initiated by excess K^+ in tissues.

Does excess K^+ induce N starvation in *A. thaliana*? The dual affinity nitrate transporter, NRT1.1 (NPF6.3/CHL1) is the main NO_3^- sensor in plant roots in addition to accounting for up to 80% of NO_3^- uptake from roots (Feng et al., 2020). Within 3 HAT and onwards, *NRT1.1* in *A. thaliana* roots is down-regulated (Fig 7A). At low soil NO_3^- levels, *NRT1.1* is activated by *CIPK23* to function as a high affinity NO_3^- transporter (Coskun et al., 2017). We note that in *A. thaliana* (and not in *S. parvula*) roots, *CIPK23* is concurrently suppressed with the main K uptake system formed of *HAK5* and *AKT1-KC1* (Fig 6C). This potentially limits the N content in roots within 24 HAT (Fig 2B) and we see *A. thaliana* roots activating N starvation signals by inducing the expression of high affinity NO_3^- transporters, *NRT2.1* and *NRT2.4* upon high K^+ treatment (Fig 7A) even when the growth medium in the current experimental condition has sufficient NO_3^- levels. NRT2.1 and NRT2.4 account for over 75% of influx when soil NO_3^- levels are low (O'Brien et al., 2016).

The long-distance transport from root to shoot via xylem loading of NO_3^- in roots is primarily regulated via NRT1.5 (NPF7.3) which is a NO_3^-/K^+ cotransporter (Li et al., 2017). We observe that in *A. thaliana* (and not in *S. parvula*) roots, *NRT1.5* is suppressed possibly in an attempt to limit excess K^+ accumulation in shoots, but consequently depriving NO_3^- in shoots (Fig 2B, Fig 7A). This high K^+ induced N starvation environment generated in *A. thaliana* is further reflected by its additional transcriptional effort to remobilize NO_3^- internally. For example, *NRT1.7* and *NRT1.8* are induced to promote translocation of NO_3^- from old to young leaves and from xylem back into roots respectively, while *NRT1.9, NRT1.11,* and *NRT1.12* are suppressed to restrict transport via phloem and limit NO_3^- movement in shoots under low NO_3^- levels (Fig 7A) (O'Brien et al., 2016). The transcriptional regulatory emphasis on *NRT1.8* is outstanding during excess K^+ stress, given that it is the highest induced (104-fold and 73-fold at 24 and 72 HAT, respectively) in the entire *A. thaliana* transcriptomic response (Fig 7A and Table S3). Even in *S. parvula* which has overall a more restrained transcriptomic response, an ortholog copy of *AtNRT1;8* is induced in roots at 24 HAT. Additionally, *NRT1.8* is triplicated in *S. parvula*

(Oh and Dassanayake, 2019), allowing additional regulatory flexibility to the species to redistribute NO_3^- via the xylem back to the roots.

NH_4^+ provides the second major source of N following NO_3^- and the growth medium provided in the current experimental conditions includes NH_4^+ at 0.2 mM compared to 1.4 mM NO_3^-. Therefore, we expected to see an induction in NH_4^+ transporters as an alternative N nutrition response to overcome the high K^+-induced N-starvation, primarily caused through the co-suppression of NO_3^- and K^+ uptake, in *A. thaliana* roots. However, there is a widely documented reciprocal antagonistic activity between NH_4^+ and K^+ transport contrasting to the interdependent cotransport activity between NO_3^- and K^+. Excess NH_4^+ limits root uptake of K^+ and its translocation to shoots and an external supply of K^+ or induction of K^+ transporters relieves ammonium toxicity (Coskun et al., 2017). Further, the high affinity NH_4^+ specific ammonium transporters (AMT) are inhibited by CIPK23 when the same is known to activate NO_3^- and K^+ transporters (Straub et al., 2017). Nonetheless, the antagonistic transport functions between NH_4^+ and K^+ are not established under excess K^+ and non-toxic NH_4^+ levels. Counterintuitive to our expectations, *AMT1;1/2/3*, which encode transporters that account for >90% of high-affinity ammonium uptake into roots (Yuan et al., 2007), were co-suppressed in *A. thaliana* concurrent to suppression of K^+ transporters that regulate soil to root influx upon excess K^+ (Fig 7A). The exception to this coordinated suppression was seen with *AMT1;5* which was induced upon high K^+ in *A. thaliana* roots (Fig 7A). Notably, *AMT1;5* has been shown to have an opposite activation mode compared to the other *AMTs* (Neuhauser et al., 2007).

We next checked whether the N assimilation pathway from NO_3^- to glutamine via NH_4^+ was also suppressed in *A. thaliana* experiencing a high K^+-induced N-starvation. Indeed, the genes coding for nitrate reductase (*NIA1/NR1, NIA2/NR2*) and nitrite reductase (*NIR*) were coordinately down-regulated in *A. thaliana* root and shoot under high K^+ (Fig 7B). In angiosperms including *A. thaliana*, the main assimilation point of inorganic N to organic compounds is the GS-GOGAT (glutamine synthetase-glutamate synthase) pathway which is tightly coupled to the N and C metabolic state of the plant (O'Brien et al., 2016). The GS enzyme coded by the *GLN* family uses NH_4^+ derived from primary N uptake; recycled from photorespiration; or remobilized from protein hydrolysis. The GOGAT enzyme comprises

plastid-targeted *GLU* and cytosolic *GLT* to form a net output of glutamate from glutamine and 2-oxoglutarate, which can be converted to various amino acids and organic acids (O'Brien et al., 2016; Ji et al., 2019). The cytosolic *GLN1;2* and plastidial *GLN2* (coding GS enzymes) together with *GLT* and *GLU1* (coding GOGAT enzymes) were suppressed under a low N and C metabolic environment created by excess K^+ (Fig 2D and 7B). Contrastingly, the induction of *GLN1;1* and *GLN1;3* together with *GLU2* especially in *A. thaliana* shoots likely reflects the transcriptional effort to recycle N under a high K^+-induced N-starved condition (Fig 7B).

We predicted that the suppression of the overall N-assimilation pathway would be reflected in the change in primary metabolite pools derived from glutamate in *A. thaliana* during excess K-induced N starvation. In our comparative transcriptome profiling, *S. parvula* boosted its transcriptional resource allocation to defend against osmotic and oxidative stresses while *A. thaliana* showed a setback in similar transcriptional efforts (Fig 5B, C and S5). We wanted to see if this setback in *A. thaliana* to mount appropriate defenses against osmotic and oxidative stress coincided with the depletion of metabolites directly derived from glutamate that are known to function as organic osmolytes and antioxidants. Proline is a primary metabolite with dual functions serving as an osmoprotectant and an antioxidant (Hayat et al., 2012). We observed a coordinated effort to accumulate proline and its immediate precursors in the induction of transcripts coding for the key proline biosynthesis enzymes (Fig 7B, *P5CS1/2*) in both species. However only *S. parvula* was able to significantly accumulate proline during exposure to excess K^+ (Fig 7C). We see similar pronounced efforts in increasing antioxidant capacity via GABA and beta-alanine (Fig 7B and C), concordant to increasing synthesis towards raffinose and myo-inositol only in *S. parvula* (Fig S3B) to protect against osmotic stress. Overall, *S. parvula* is not hindered in its capacity to accumulate carbon and nitrogen-rich antioxidants and osmoprotectants by maintaining N uptake from roots and N-assimilation pathways separated from the suppressed K-uptake pathways. Contrastingly, the two processes were jointly suppressed in *A. thaliana* leading to the depleted N resources (Fig. 2B) and, in turn, failure to accumulate C and N-rich protective metabolites (Fig 7C).

Co-expressed gene clusters between *S. parvula* and *A. thaliana* indicate stress preparedness in *S. parvula*

Given the more targeted transcriptomic responses (Fig 5) and its niche adaptations to survive high K^+ levels found in its native habitat (Oh et al., 2014), we predicted that, in *S. parvula*, a large proportion of stress adapted transcripts would be constitutively expressed, as previously reported for stress preparedness at the basal level for B toxicity (Wang et al., 2021). To deduce constitutively expressed transcripts in *S. parvula* with decisive roles in preadaptation toward high K^+, we generated co-expressed ortholog pair clusters using 14,318 and 14,903 ortholog pairs expressed in root and shoot respectively, in *A. thaliana* and *S. parvula*. Among them, we identified five root and three shoot co-expressed clusters (Fig 8, RC1-5 and SC1-3, respectively) that had significant basal expression differences and high K^+ stress transcriptomic responses significantly regulated only in one of the species, a pattern that may signify stress-prepared transcriptomes unique to each species (Fig 8 and Table S11).

In three out of five root co-expression clusters, only *A. thaliana* orthologs showed induction or suppression with a maximum response at 24 HAT (Fig 8A, RC1-3). These clusters largely represented transcripts associated with stress responses, C and N metabolism, transport, and root development we discussed earlier (Fig 4). Interestingly, the 4th and 5th clusters (Fig 8A, RC4-5) of which *S. parvula* showed a response, accounted for 203 ortholog pairs. Yet, 37% of these orthologs had no functional annotations that could be deduced from Gene Ontologies and therefore could not be meaningfully summarized into representative processes. This highlights the extent of functional obscurity or novelty of genes that respond to specific ionic stresses even in *A. thaliana* (Fig 8A, RC5), and the novel regulatory modes detected in orthologs of closely related species whose functional assignment may have been overlooked due to the lack of responses in the model plant *A. thaliana* (Fig 8A, RC4). In all three shoot co-expressed clusters, *A. thaliana* showed a response that peaked at 24 HAT, while the *S. parvula* orthologs showed a constitutive expression either lower than the basal level in *A. thaliana* (Fig 8B, SC1), higher than the induced level in *A. thaliana* (Fig 8B, SC2), or equaled the control (0 HAT) level in *A. thaliana* (Fig 8B, SC3). The enriched functions in shoot clusters largely overlapped to include stress responses and C and N metabolic processes. In all, 9836 ortholog pairs, all clusters except RC4 and RC5, showed constitutive expression in *S. parvula* while only 76 ortholog pairs (RC4) showed a unique response from *S. parvula* when *A. thaliana* showed

constitutive expression (Fig 8). Overall, these co-expressed clusters between *A. thaliana* and *S. parvula* demonstrate the stability in transcriptional resource allocation (*i.e.* stress preparedness) in *S. parvula* to facilitate growth and development during excess K^+ stress, while significant alterations are observed for *A. thaliana* orthologs coinciding with its growth interruptions during high K^+ stress and erratic transcriptional resource management.

Discussion

Salt stress mechanisms induced by high K^+ is largely unknown compared to the collective understanding for high Na^+ tolerance in plants. Our results demonstrate that high K^+ is more detrimental to plants than Na^+ given at the same external concentrations (Fig 1). Previous studies support this observation noting that excess KCl caused more severe salt stress symptoms than NaCl in multiple crops and even among halophytes (Eijk, 1939; Ashby and Beadle, 1957; Eshel, 1985; Matoh et al., 1986; Cramer et al., 1990; Wang et al., 2001; Ramos et al., 2004; Richter et al., 2019). Generally, halophytes have evolved to survive high levels of Na and the subsequent toxicity symptoms entailing oxidative, osmotic, and ionic stresses, while being able to uptake K (Kazachkova et al., 2018; Pantha and Dassanayake, 2020). However, the canonical adaptations described for salt tolerance mechanisms associated with NaCl-induced salt stress are insufficient to explain adaptations required for KCl-induced salt stress.

The molecular mechanisms underlying K^+ toxicity, excess K^+ sensing, and how those signals are transduced to manage overall stress avoidance or mitigation had been hardly investigated in plants. The extremophyte model, *S. parvula,* amidst high K^+ at growth unfavorable levels can sustain its growth and development; compartmentalize excess K more in roots than in shoots; maintain uninterrupted nutrient uptake; increase its antioxidant and osmoprotectant pools; decouple transcriptional regulation between K and N uptake; and coordinately induce abiotic stress response pathways along with growth promoting pathways (Fig 9). Contrastingly, the more stress-sensitive plant, *A. thaliana*, shows interrupted root and shoot growth; excessive accumulation of K^+ in both roots and shoots; depletion of essential nutrients; depletion of N-containing primary metabolites; and sweeping transcriptomic adjustments suggesting initiation of autophagy, ROS accumulation, response to both abiotic

and biotic stresses, and responses to all major hormone pathways (Fig 9). We propose two deterministic steps in the overall stress response sequence exhibited by *A. thaliana* as critical flaws to survive high K^+ stress of which *S. parvula* shows efficient stress management responses that allows it to survive KCl-induced salt stress.

Surviving high K toxicity by avoiding N starvation

Unlike in *A. thaliana,* even when excess K^+ was accumulating in *S. parvula* roots over time, the overall root growth was not severely affected and nutrient balance was maintained (Fig 1 and 2). Halophytes are known for their capability to maintain nutrient balance and prevent excess salt from accumulating in shoots under salt stresses exerted by NaCl (Kazachkova et al., 2018; Zhao et al., 2020). However, unlike Na, K is a macronutrient and plants have evolved many more functionally redundant transporters to uptake K^+ into roots and redistribute into shoots via xylem and phloem (Shabala and Cuin, 2008). When external K^+ levels exceed physiologically optimal conditions, it is not surprising that the immediate response from both plants was to suppress expression of selective K^+ transporters that primarily control K^+ influx known to operate at the root soil interface (Fig 6). Additionally, *S. parvula* further down-regulates non-selective CNGC cation channels that may be permeable to K^+ especially in roots. Several CNGC type channels are reported to allow Na^+ or K^+ transport and have been implicated in their functions during Na-induced salt stress by controlling Na influx into roots. However, their functional and spatiotemporal specificity remains largely unresolved (Dietrich et al., 2020) and needs to be determined before evaluating how selected CNGCs may be involved in also limiting excess K flow into roots under K-induced salt stress.

Concurrent to suppression of K^+ uptake, *A. thaliana* co-suppresses long distance transport of K^+, presumably to limit K accumulation in shoots. One of the key transporters used in this process is NRT1.5 which is a co-transporter of NO_3^- and K^+ (Li et al., 2017). NO_3^- is transported as a counterion with K^+ in plant root to shoot translocation as described by the 'Dijkshoorn–Ben Zioni model' (Dijkshoorn et al., 1968; Zioni et al., 1971; Coskun et al., 2017). The suppression of *NRT1.5* limits NO_3^- remobilization in plants (Chen et al., 2012). This obstruction to N transport within the plant is compounded by the transcriptional co-suppression of NRT and AMT transporters known to operate at the root soil interface limiting N

intake into plants (Fig 7) (Tegeder and Masclaux-Daubresse, 2018). This creates an N-starved condition for *A. thaliana* not observed for *S. parvula.* During limiting K^+ conditions, N-uptake is down regulated to prevent excess N-induced toxicity in plants as a favorable mechanism to adapt to K^+ starvation (Armengaud et al., 2004). This interdependent co-transport and regulation between N and K that is favorable at low K^+ levels appear to be detrimental at high K^+ levels as it functions as an antagonistic pleiotropic effect.

We observe a significant transcriptional level effort in *A. thaliana* to induce *NRT1.8/NPF7.2* (the most induced gene in *A. thaliana* during excess K^+ stress) and thereby avoid N depletion in roots by N-reimport from the stele (Li et al., 2010). However, this transcriptional effort did not cascade to the ionomic level (Fig 2B, D, and E). N remobilization via induction of *NRT1.8* while concurrently suppressing *NRT1.5* (Fig 7A) during N starvation is regulated by ethylene-jasmonic acid signaling together with low N-sensing by nitrate reductase (Chen et al., 2012; Zhang et al., 2014). Both ethylene and jasmonic acid signaling are among the enriched differently regulated transcriptional processes in *A. thaliana* (Fig 4B). Interestingly, *S. parvula* appears to have a more flexible and effective regulatory capacity to allow N-uptake decoupled from restricted K-uptake and also it does not suppress internal remobilization of NO_3^- and K^+ via NRT1.5 (Fig 6 and 7). This frees *S. parvula* from experiencing a high-K induced N-starvation.

The depletion of N uptake in *A. thaliana* further descends into depletion of primary metabolic pools rich in N (Fig 3D) with a concomitant transcriptional suppression observed in N assimilation via the GS-GOGAT pathway (Fig 7) (O'Brien et al., 2016; Ji et al., 2019). This not only creates a shortage of essential primary metabolic pools required for growth and development, but also depletes essential antioxidant and osmolyte pools to defend against the mounting oxidative and osmotic stresses (Fig 3, 7, 9). K is known to exert osmotic stress at a comparable level to Na and high K can also lead to oxidative damage (Osakabe et al., 2013; Zheng et al., 2013). This creates an overall need to boost osmotic and antioxidant defense systems to successfully survive high K^+ toxicity stress.

Accumulation of compatible osmolytes during osmotic stress reduces water loss from tissues and helps to maintain turgor pressure which in turn would allow plants to regulate water transport and photosynthesis (Apse and Blumwald, 2000). Synergistic transcriptional and

metabolic resource allocation to increase osmoprotectants during high K^+ stress is much more pronounced in *S. parvula* than in *A. thaliana*. Among several osmolytes highlighted in our results earlier, *S. parvula* roots and shoots notably accumulated significantly higher levels of proline. Further, its precursors, glutamine and glutamate, were also highly accumulated in *S. parvula* root (Fig 3 and 7). Stress tolerance upon increased accumulation of proline resulting from both increased synthesis and reduced catabolism has been previously shown as a key adaptive mechanism in *E. salsugineum* during salt stress, an extremophyte relative of *S. parvula* (Kant et al., 2006). Proline plays an important role by serving as an osmolyte, and an antioxidant, and is reported to facilitate increased photosynthesis during salt stress in many plants (Kishor et al., 1995; Gong et al., 2005; Kumar et al., 2010; Ghanti et al., 2011; Hayat et al., 2012).

K and N together and independently regulate phosphorus (P) uptake into plants (Coskun et al., 2017; Maeda et al., 2018; Cui et al., 2019). Additionally, high K^+ toxicity has been reported to induce P-starvation (Ródenas et al., 2019). Therefore, K and N status of a plant serve as a key determinant that controls the overall nutrient uptake processes including P uptake in plants and availability of defense compounds required during salt stress. During high K-induced N-starved conditions, *A. thaliana* experienced severe shortages of multiple key nutrients (Fig 2), which *S. parvula* seemingly avoided by having independent regulatory capacity of K and N uptake and remobilization (Fig 6, 7, and 9). Therefore, we propose that the ability to regulate independent K^+ uptake is the first key deterministic step towards building resilience to high external K^+.

Efficient transcriptional resource allocation vs transcriptional mismanagement

Pleiotropic K signaling beneficial under low K conditions lead to wasteful transcriptional resources during high K^+ conditions in *A. thaliana* and leads to futile activation of multiple hormone signaling pathways. K serves as a key signaling molecule for hormonal regulation required for developmental processes, biotic stress signaling, and abiotic stress signaling (Zhang et al., 2014; Hauser et al., 2017; Shabala, 2017; Hughes et al., 2020; Hetherington et al., 2021). Plants constantly sense and adjust growth and development based on nutrient availability, and in the context of K availability, all canonical mechanisms described for hormone-dependent

growth modifications that involve sensing K^+ are based on sensing external K^+ at low or growth favorable conditions. When supplied with toxic levels of K^+ for most plants, we found that *A. thaliana* was unable to adjust the K-dependent signaling to fit the extant specific stress condition and allowed non- selective hormone signaling pathways to be transcriptionally regulated (Fig 4). This would have led to transcriptional resource mismanagement especially when biotic stress response pathways were activated concurrent to depleted N-sources and when it was at a comparable level of proportional allocation assigned to abiotic stress management (Fig 2, 3, 4B, 5, and S5). This level of non-selective transcriptional activity is indicative of transcriptional mismanagement in *A. thaliana* seen at 24 HAT and it is not a signature of deregulation or lack of regulation expected from dying plants as we observe a clear decline in such non-selective pathway regulation by 72 HAT of exposure to high K^+ (Fig 4B). Therefore, we propose that the capacity to avoid non-selective transcriptional mismanagement is the second major deterministic step in surviving high K^+ stress. If unavoided, it can lead to systemic damage via activation of ROS and autophagy pathways, as demonstrated by *A. thaliana* with its increased ROS accumulation perhaps resulting from induction of biotic stress responses or unmitigated oxidative stresses directly induced by high K^+ detrimental especially at a nutrient starved environment created by high K^+ (Fig 4). ROS signals are known to induce autophagy often associated with abiotic and biotic stress responses, and during nutrient recycling, in addition to several plant developmental processes (Liu et al., 2005; Thompson et al., 2005; Lv et al., 2014; Pantha and Dassanayake, 2020). However, uncontrolled or misregulated initiation of autophagy signifies a failed stress response strategy (Floyd et al., 2015). In *A. thaliana* shoots, autophagy is the most enriched transcriptional pathway active at 24 and 72 HAT. The collective transcriptional signal enriched for pathways associated with lipid catabolism, protein degradation, DNA repair, cell death, and leaf senescence (Das and Roychoudhury, 2014) (Fig 4B) is further indicative of the maladaptive stress response strategies shown by *A. thaliana* contrasted against *S. parvula* which shows a more refined transcriptional response to survive high K^+ stress. The *S. parvula* transcriptome shows a pre-adapted state to high K^+ stress when examined together with co-expressed orthologs in *A. thaliana. S. parvula* mostly activates a limited yet focused response towards achieving stress tolerance while

supporting overall growth and metabolism (Fig 5 and 8). Extremophyte transcriptomes and metabolomes including previous reports on *S. parvula* have shown similar stress-ready states constant stresses frequently associated with their native environments (Kant et al., 2006; Lugan et al., 2010; Oh et al., 2014; Lee et al., 2021; Wang et al., 2021).

In conclusion, upon exposure to high K^+, plants undergo physiological, metabolic, and transcriptional changes and a subset of those changes lead to stress adaptive traits while the other responses are indicative of failed cellular responses unable to meet the increasing systemic stress exerted by excess K^+ retention in tissues. The deterministic step whether a plant would be able to survive K-induced salt stress or descend into unmitigated stress responses was primarily set early on in the ability to regulate K uptake independent from other nutrient uptake pathways. This decoupled regulation of K sensing and stress signaling can be leveraged to design improved crops that are better able to dynamically adjust to a wide array of soils or irrigation water sources with different salt compositions.

Acknowledgements

We thank Dr. Guannan Wang, Kieu-Nga Tran, Chathura Wijesinghege, Dr. Aaron Smith, and Dr. John Larkin for providing feedback on the manuscript and facilitating helpful discussions; Prava Adhikari for additional assistance with phenotyping, and undergraduate students Saad Chaudhari, Megan Guilbeau, and August Steinkamp for their assistance to grow plants. This work was supported by the US National Science Foundation awards MCB-1616827 and IOS-EDGE-1923589, US Department of Energy BER-DE-SC0020358, and the Next-Generation BioGreen21 Program of Republic of Korea (PJ01317301) awarded to MD and DHO. PP was supported by an Economic Development Assistantship award from Louisiana State University. We acknowledge the LSU High Performance Computing services for providing computational resources needed for data analyses.

Author Contributions

PP conducted experiments and performed data analyses. DL supervised and assisted with measuring CO_2 assimilation rates. DHO provided bioinformatics assistance. MD developed the

experimental design and supervised the overall project. PP and MD interpreted results and wrote the article with input from all co-authors who revised and approved the final manuscript.

References

Ali A, Khan IU, Jan M, Khan HA, Hussain S, Nisar M, Chung WS, Yun D-J (2018) The High-Affinity Potassium Transporter EpHKT1;2 From the Extremophile Eutrema parvula Mediates Salt Tolerance. Front Plant Sci **9**: 1–11

Ali A, Raddatz N, Aman R, Kim S, Park HC, Jan M, Baek D, Khan IU, Oh D, Lee SY, et al (2016) A Single Amino-Acid Substitution in the Sodium Transporter HKT1 Associated with Plant Salt Tolerance. Plant Physiol **171**: 2112–2126

Andrews S (2010) FastQC: A quality control tool for high throughput sequence data. Babraham Bioinforma http://www.bioinformatics.babraham.ac.uk/projects/

Apse MP, Blumwald E (2000) Engineering salt tolerance in plants. Curr Opin Biotechnol **13**: 146–150

Aquea F, Federici F, Moscoso C, Vega A, Jullian P, Haseloff J, Arce-Johnson P (2012) A molecular framework for the inhibition of Arabidopsis root growth in response to boron toxicity. Plant, Cell Environ **35**: 719–734

Arienzo M, Christen EW, Quayle W, Kumar A (2009) A review of the fate of potassium in the soil-plant system after land application of wastewaters. J Hazard Mater **164**: 415–422

Armengaud P, Breitling R, Amtmann A (2004) The Potassium-Dependent Transcriptome of Arabidopsis Reveals a Prominent Role of Jasmonic Acid in Nutrient Signaling. Plant Physiol **136**: 2556–2576

Ashby WC, Beadle NCW (1957) Studies in Halophytes : III . Salinity Factors in the Growth of Australian Saltbushes Author (s): W . C . Ashby and N . C . W . Beadle Published by : Wiley on behalf of the Ecological Society of America Stable URL : https://www.jstor.org/stable/1931695. Ecology **38**: 344–352

Ashley MK, Grant M, Grabov A (2006) Plant responses to potassium deficiencies: a role for potassium transport proteins. J Exp Bot **57**: 425–436

Bassil E, Zhang S, Gong H, Tajima H, Blumwald E (2019) Cation specificity of vacuolar NHX-type cation/H + Antiporters 1. Plant Physiol **179**: 616–629

Baxter IR, Ziegler G, Lahner B, Mickelbart M V, Foley R, Danku J, Armstrong P, Salt DE, Hoekenga OA (2014) Single-Kernel Ionomic Profiles Are Highly Heritable Indicators of Genetic and Environmental Influences on Elemental Accumulation in Maize Grain (Zea mays). PLoS One. doi: 10.1371/journal.pone.0087628

Chen CZ, Lv XF, Li JY, Yi HY, Gong JM (2012) Arabidopsis NRT1.5 is another essential component in the regulation of nitrate reallocation and stress tolerance. Plant Physiol **159**: 1582–1590

Conway JR, Lex A, Gehlenborg N (2017) UpSetR : an R package for the visualization of intersecting sets and their properties. **33**: 2938–2940

Coskun D, Britto DT, Kronzucker HJ (2017) The nitrogen–potassium intersection: membranes, metabolism, and mechanism. Plant Cell Environ **40**: 2029–2041

Cramer GR, Epstein E, Lauchli A (1990) Effects of sodium , potassium and calcium on salt-stressed barley . I . Growth analysis. 83–88

Cui Y, Li X, Yuan J, Wang F, Wang S (2019) Biochemical and Biophysical Research Communications Nitrate transporter NPF7 . 3 / NRT1 . 5 plays an essential role in regulating phosphate de fi ciency responses in Arabidopsis. Biochem Biophys Res Commun **508**: 314–319

Das K, Roychoudhury A (2014) Reactive oxygen species (ROS) and response of antioxidants as ROS-scavengers during environmental stress in plants. Front Environ Sci **2**: 1–13

Dassanayake M, Oh D-H, Haas JS, Hernandez A, Hong H, Ali S, Yun D-J, Bressan R a, Zhu J-K, Bohnert HJ, et al (2011) The genome of the extremophile crucifer Thellungiella parvula. Nat Genet **43**: 913–918

Daudi A, O'Brien JA (2012) Detection of Hydrogen Peroxide by DAB Staining in. Bio-protocol **2**: e263

Demidchik V, Straltsova D, Medvedev SS, Pozhvanov GA, Sokolik A (2014) Stress-induced electrolyte leakage : the role of K+ -permeable channels and involvement in programmed cell death and metabolic adjustment. J Exp Bot **65**: 1259–1270

Dietrich P, Moeder W, Yoshioka K (2020) Plant cyclic nucleotide-gated channels: New insights on their functions and regulation. Plant Physiol **184**: 27–38

Dijkshoorn W, Lathwell DJ, Wit CTDE (1968) Temporal changes in carboxylate content of ryegrass with stepwise change in nutrition. Plant Soil

Dreyer I, Gomez-Porras JL, Riedelsberger J (2017) The potassium battery: a mobile energy source for transport processes in plant vascular tissues. New Phytol **216**: 1049–1053

Duval JS, Carson JM, Holman PB, Darnley AG (2005) Terrestrial Radioactivity and Gamma-ray Exposure in the United States and Canada. US Geol Surv Open-File Rep 1413:

Eijk VM (1939) Analysis of the effect of NaCl on development, succulence and transpiration in Salicornia herbacea, as well as studies on the influence of salt uptake on root respiration in Aster Tripolium. Recl des Trav Bot néerlandais **36**: 559–657

Eshel A (1985) Response of Suaeda aegyptiaca to KCl, NaCl and Na2SO4 treatments. Physiol Plant **64**: 308–315

Feng H, Fan X, Miller AJ, Xu G (2020) Plant nitrogen uptake and assimilation: Regulation of cellular pH homeostasis. J Exp Bot **71**: 4380–4392

Ferreira T, Rasband W (2012) ImageJ User Guide User Guide ImageJ.

Fiehn O, Wohlgemuth G, Scholz M, Kind T, Lee DY, Lu Y, Moon S, Nikolau B (2008) Quality control for plant metabolomics: Reporting MSI-compliant studies. Plant J **53**: 691–704

Floyd BE, Pu Y, Soto-Burgos J, Bassham DC (2015) To Live or Die: Autophagy in Plants. In: Gunawardena A., McCabe P. (eds) Plant Programmed Cell Death. Springer, Cham

Gasch AP, Eisen MB (2002) Exploring the conditional coregulation of yeast gene expression through fuzzy k-means clustering. Genome Biol. doi: 10.1186/gb-2002-3-11-research0059

Gaymard F, Pilot G, Lacombe B, Bouchez D, Bruneau D, Boucherez J, Michaux-Ferrière N, Thibaud JB, Sentenac H (1998) Identification and disruption of a plant shaker-like outward channel involved in K+release into the xylem sap. Cell **94**: 647–655

Ghanti SKK, Sujata KG, Kumar BMV, Karba NN (2011) Heterologous expression of P5CS gene in chickpea enhances salt tolerance without affecting yield. Biol Plant **55**: 634–640

Gierth M, Mäser P, Schroeder JI (2005) The potassium transporter AtHAK5 functions in K(+) deprivation-induced high-affinity K(+) uptake and AKT1 K(+) channel contribution to K(+) uptake kinetics in Arabidopsis roots. Plant Physiol **137**: 1105–14

Gobert A, Isayenkov S, Voelker C, Czempinski K, Maathuis FJM (2007) The two-pore channel TPK1 gene encodes the vacuolar K ⁒ conductance and plays a role in K ⁒ homeostasis. Proc Natl Acad Sci USA **104**: 10726–10731

Gobert A, Park G, Amtmann A, Sanders D, Maathuis FJM (2006) Arabidopsis thaliana Cyclic Nucleotide Gated Channel 3 forms a non-selective ion transporter involved in germination and cation transport. J Exp Bot **57**: 791–800

Gong Q, Li P, Ma S, Indu Rupassara S, Bohnert HJ (2005) Salinity stress adaptation competence in the extremophile *Thellungiella halophila* in comparison with its relative *Arabidopsis thaliana*. Plant J **44**: 826–839

Gu Z, Gu L, Eils R, Schlesner M, Brors B (2014) circlize implements and enhances circular visualization in R. Bioinformatics **30**: 2811–2812

Guo K, Babourina O, Christopher DA, Borsics T, Rengel Z (2008) The cyclic nucleotide-gated channel, AtCNGC10, influences salt tolerance in Arabidopsis. Physiol Plant **134**: 499–507

Han M, Wu W, Wu WH, Wang Y (2016) Potassium Transporter KUP7 Is Involved in K+ Acquisition and Translocation in Arabidopsis Root under K+-Limited Conditions. Mol Plant **9**: 437–446

Hauser F, Li Z, Waadt R, Schroeder JI (2017) SnapShot: Abscisic Acid Signaling. Cell **171**: 1708-1708.e0

Hayat S, Hayat Q, Alyemeni MN, Wani AS, Pichtel J, Ahmad A, Hayat S, Hayat Q, Alyemeni MN, Wani AS, et al (2012) Role of proline under changing environments A review Role of proline under changing environments A review. doi: 10.4161/psb.21949

Hetherington FM, Kakkar M, Topping JF, Lindsey K (2021) Gibberellin signaling mediates lateral root inhibition in response to K+ -deprivation. Plant Physiol **185**: 1198–1215

Hughes AM, Zwack PJ, Cobine PA, Rashotte AM (2020) Cytokinin-regulated targets of Cytokinin Response Factor 6 are involved in potassium transport. Plant Direct 1–15

IPCC (2019) Climate Change and Land: an IPCC special report on climate change, desertification, land degradation, sustainable land management, food security, and greenhouse gas fluxes in terrestrial ecosystems [P.R. Shukla, J. Skea, E. Calvo Buendia, V. Masson-De.

Ivashikina N, Dirk B, Ache P, Meyerho O, Felle HH, Hedrich R (2001) K+ channel profile and electrical properties of Arabidopsis root hairs. FEBS Lett **508**: 463–469

Jabs T, Dietrich RA, Dangl JL (1996) Initiation of runaway cell death in an Arabidopsis mutant by extracellular superoxide. Science (80-) **273**: 1853–1856

Ji Y, Li Q, Liu G, Selvaraj G, Zheng Z, Zou J, Wei Y (2019) Roles of Cytosolic Glutamine Synthetases in Arabidopsis Development and Stress Responses. Plant Cell Physiol **60**: 657–671

Kanehisa M, Sato Y, Kawashima M, Furumichi M, Tanabe M (2016) KEGG as a reference resource for gene and protein annotation. Nucleic Acids Res **44**: D457–D462

Kant S, Kant P, Raveh E, Barak S (2006) Evidence that differential gene expression between the halophyte, Thellungiella halophila, and Arabidopsis thaliana is responsible for higher levels of the compatible osmolyte proline and tight control of Na+ uptake in T. halophila. Plant, Cell Environ **29**: 1220–1234

Kazachkova Y, Eshel G, Pantha P, Cheeseman JM, Dassanayake M, Barak S (2018) Halophytism: What Have We Learnt From Arabidopsis Relative Model Systems? Plant Physiol **178**: 972–988

Kim MJ, Ruzicka D, Shin R, Schachtman DP (2012) The Arabidopsis AP2 / ERF Transcription Factor RAP2 . 11 Modulates Plant Response to Low-Potassium Conditions. Mol Plant **5**: 1042–1057

Kishor PBK, Hong Z, Miao C-H, Hu C-AA, Verma DPS (1995) Overexpression of A1-Pyrroline-5-Carboxylate Synthetase lncreases Proline Production and Confers Osmotolerance in Transgenic Plants ’. Plant Physiol **108**: 1387–1394

Kolde R (2012) pheatmap v.1.0.8. https://cran.r-project.org/package=pheatmap 1–7

Kumar V, Shriram V, Kishor PBK (2010) Enhanced proline accumulation and salt stress tolerance of transgenic indica rice by over-expressing P5CSF129A gene. Plant Biotechnol Rep **4**: 37–48

Langmead B, Trapnell C, Pop M, Salzberg SL (2009) Ultrafast and memory-efficient alignment of short DNA sequences to the human genome. Genome Biol **10**: R25

Lee G, Ahmadi H, Quintana J, Syllwasschy L, Preite V, Anderson JE, Genetics M, Information C, Footnotes A (2021) Constitutively enhanced genome integrity maintenance and direct stress mitigation characterize transcriptome of extreme stress-adapted Arabidopsis halleri. bioRxiv

Leigh R, Wyn Jones RG (1984) A hypothesis relating critical potassium concentrations for growth to the distribution and function of this ion in the plant cell. New Phytol. 97. 1–13

Lequeux H, Hermans C, Lutts S, Verbruggen N (2010) Response to copper excess in Arabidopsis thaliana: Impact on the root system architecture, hormone distribution, lignin accumulation and mineral profile. Plant Physiol Biochem **48**: 673–682

Li H, Yu M, Du XQ, Wang ZF, Wu WH, Quintero FJ, Jin XH, Li HD, Wang Y (2017) NRT1.5/NPF7.3 functions as a proton-coupled H+/K+ antiporter for K+ loading into the xylem in arabidopsis. Plant Cell **29**: 2016–2026

Li JY, Fu YL, Pike SM, Bao J, Tian W, Zhang Y, Chen CZ, Zhang Y, Li HM, Huang J, et al (2010) The Arabidopsis nitrate transporter NRT1.8 functions in nitrate removal from the xylem sap and mediates cadmium tolerance. Plant Cell **22**: 1633–1646

Liu Y, Schiff M, Czymmek K, Tallóczy Z, Levine B, Dinesh-Kumar SP (2005) Autophagy regulates programmed cell death during the plant innate immune response. Cell **121**: 567–577

Love MI, Huber W, Anders S (2014) Moderated estimation of fold change and dispersion for RNA-seq data with DESeq2. Genome Biol **15**: 550

Lugan R, Niogret MF, Leport L, Guégan JP, Larher FR, Savouré A, Kopka J, Bouchereau A (2010) Metabolome and water homeostasis analysis of Thellungiella salsuginea suggests that dehydration tolerance is a key response to osmotic stress in this halophyte. Plant J **64**: 215–229

Lv X, Pu X, Qin G, Zhu T, Lin H (2014) The roles of autophagy in development and stress responses in Arabidopsis thaliana. Apoptosis **19**: 905–921

Maathuis FJ (2009) Physiological functions of mineral macronutrients. Curr Opin Plant Biol **12**: 250–258

Maeda Y, Konishi M, Kiba T, Sakuraba Y, Sawaki N, Kurai T, Ueda Y, Sakakibara H, Yanagisawa S (2018) A NIGT1-centred transcriptional cascade regulates nitrate signalling and incorporates phosphorus starvation signals in Arabidopsis. Nat Commun. doi: 10.1038/s41467-018-03832-6

Maere S, Heymans K, Kuiper M (2005) BiNGO: A Cytoscape plugin to assess overrepresentation

of Gene Ontology categories in Biological Networks. Bioinformatics **21**: 3448–3449

Matoh T, Watanabe J, Takahashi E (1986) Effects of Sodium and Potassium Salts on the Growth of a Halophyte. Soil Sci Plant Nutr **32**: 451–459

Murashige T, Skoog F (1962) A Revised Medium for Rapid Growth and Bio Assays with Tobacco Tissue Cultures. Physiol Plant **15**: 473–497

Neuhauser B, Dynowski M, Mayer M, Ludewig U (2007) Regulation of NH 4 1 Transport by Essential Cross Talk between AMT Monomers through the. Plant Physiol **143**: 1651–1659

Nilhan TG, Emre YA, Osman K (2008) Soil Determinants for distribution of Halocnemum strobilaceum Bieb. (Chenopodiaceae)Around Lake Tuz, Turkey. Pakistan J Biol Sci **11**: 565–570

Nishizawa A, Yabuta Y, Shigeoka S (2008) Galactinol and Raffinose Constitute a Novel Function to Protect Plants from Oxidative Damage. Plant Physiol **147**: 1251–1263

O'Brien JAA, Vega A, Bouguyon E, Krouk G, Gojon A, Coruzzi G, Gutiérrez RAA (2016) Nitrate Transport, Sensing, and Responses in Plants. Mol Plant **9**: 837–856

Oh D-H, Dassanayake M (2019) Landscape of gene transposition-duplication within the Brassicaceae family. DNA Res **26**: 21–36

Oh D-H, Hong H, Lee SY, Yun D-J, Bohnert HJ, Dassanayake M (2014) Genome structures and transcriptomes signify niche adaptation for the multi-ion tolerant extremophyte *Schrenkiella parvula*. Plant Physiol **164**: 2123–2138

Oh D-H, Leidi E, Zhang Q, Hwang S-M, Li Y, Quintero FJ, Jiang X, D'Urzo MP, Lee SY, Zhao Y, et al (2009) Loss of halophytism by interference with SOS1 expression. Plant Physiol **151**: 210–22

Osakabe Y, Arinaga N, Umezawa T, Katsura S, Nagamachi K, Tanaka H, Ohiraki H, Yamada K, Seo S-U, Abo M, et al (2013) Osmotic Stress Responses and Plant Growth Controlled by Potassium Transporters in Arabidopsis. Plant Cell **25**: 609–624

Pantha P, Chalivendra S, Oh DH, Elderd BD, Dassanayake M (2021) A tale of two transcriptomic responses in agricultural pests via host defenses and viral replication. Int J Mol Sci **22**: 1–27

Pantha P, Dassanayake M (2020) Living with Salt. Innov **1**: 100050

Ragel P, Ródenas R, García-martín E, Andrés Z, Villalta I, Nieves-cordones M, Rivero RM, Martínez V, Pardo JM, Quintero FJ, et al (2015) The CBL-Interacting Protein Kinase CIPK23 Regulates HAK5-Mediated High-Af fi nity K + Uptake in Arabidopsis Roots 1 [OPEN]. Plant Physiol **169**: 2863–2873

Ramos J, López MJ, Benlloch M (2004) Effect of NaCl and KCl salts on the growth and solute accumulation of the halophyte Atriplex nummularia. Plant Soil **259**: 163–168

Richter JA, Behr JH, Erban A, Kopka J, Zörb C (2019) Ion-dependent metabolic responses of Vicia faba L. to salt stress. Plant Cell Environ **42**: 295–309

Ródenas R, Martinez V, Nieves-cordones M, Rubio F (2019) High External K + Concentrations Impair Pi Nutrition , Induce the Phosphate Starvation Response , and Reduce Arsenic Toxicity in Arabidopsis Plants. Int J Mol Sci **20**: 1–18

Shabala S (2017) Signalling by potassium: Another second messenger to add to the list? J Exp Bot **68**: 4003–4007

Shabala S, Cuin TA (2008) Potassium transport and plant salt tolerance. Physiol Plant **133**: 651–669

Shi H, Ishitani M, Kim C, Zhu J-K (2000) The Arabidopsis thaliana salt tolerance gene SOS1

encodes a putative Na+/H+ antiporter. Proc Natl Acad Sci USA **97**: 6896–6901

Srivastava AK, Penna S, Nguyen D Van, Tran LP (2014) Multifaceted roles of aquaporins as molecular conduits in plant responses to abiotic stresses. Crit Rev Biotechnol **8551**: 1–10

Straub T, Ludewig U, Neuhäuser B (2017) The Kinase CIPK23 Inhibits Ammonium Transport in Arabidopsis thaliana. Plant Cell **29**: 409–422

Szyroki A, Ivashikina N, Dietrich P, Roelfsema MRG, Ache P, Reintanz B, Deeken R, Godde M, Felle H, Steinmeyer R, et al (2001) KAT1 is not essential for stomatal opening. Proc Natl Acad Sci U S A **98**: 2917–2921

Taji T, Ohsumi C, Iuchi S, Seki M, Kasuga M, Kobayashi M, Yamaguchiâ€Shinozaki K, Shinozaki K (2002) Important roles of drought- and cold-inducible genes for galactinol synthase in stress tolerance in Arabidopsis thaliana. Plant J **29**: 417–426

Takahashi F, Shinozaki K (2019) Long-distance signaling in plant stress response. Curr Opin Plant Biol **47**: 106–111

Tegeder M, Masclaux-Daubresse C (2018) Source and sink mechanisms of nitrogen transport and use. New Phytol **217**: 35–53

Thompson AR, Doelling JH, Suttangkakul A, Vierstra RD (2005) Autophagic Nutrient Recycling in Arabidopsis Directed by the ATG8 and ATG12 Conjugation Pathways 1. Plant Physiol **138**: 2097–2110

Uozumi N, Kim EJ, Rubio F, Yamaguchi T, Muto S, Tsuboi a, Bakker EP, Nakamura T, Schroeder JI (2000) The Arabidopsis HKT1 gene homolog mediates inward Na(+) currents in xenopus laevis oocytes and Na(+) uptake in Saccharomyces cerevisiae. Plant Physiol **122**: 1249–1259

Voelker C, Schmidt D, Mueller-roeber B, Czempinski K (2006) Members of the Arabidopsis AtTPK / KCO family form homomeric vacuolar channels in planta. Plant J **48**: 296–306

Wang B, Lüttge U, Ratajczak R (2001) Effects of salt treatment and osmotic stress on V-ATPase and V-PPase in leaves of the halophyte Suaeda salsa. J Exp Bot **52**: 2355–2365

Wang G, DiTusa SF, Oh DH, Herrmann AD, Mendoza-Cozatl DG, O'Neill MA, Smith AP, Dassanayake M (2021) Cross species multi-omics reveals cell wall sequestration and elevated global transcription as mechanisms of boron tolerance in plants. New Phytol. doi: 10.1101/2020.10.01.321760

Wang G, Oh D, Dassanayake M (2020) GOMCL: a toolkit to cluster, evaluate, and extract non-redundant associations of Gene Ontology-based functions. BMC Bioinformatics **21**: 1–9

Wang X-P, Li-MeiChen, Liu W-X, Shen L-K, Wang F-L, Zhou Y, Zhang Z, Wu W-H, Wang Y (2016) AtKC1 and CIPK23 Synergistically Modulate AKT1-Mediated Low-Potassium Stress. Plant Physiol **170**: 2264–2277

Wang Y, Wu W-H (2013) Potassium Transport and Signaling in Higher Plants. Annu Rev Plant Biol **64**: 451–476

Xu J, Li HD, Chen LQ, Wang Y, Liu LL, He L, Wu WH (2006) A Protein Kinase, Interacting with Two Calcineurin B-like Proteins, Regulates K+ Transporter AKT1 in Arabidopsis. Cell **125**: 1347–1360

Yoshitake Y, Nakamura S, Shinozaki D, Izumi M (2021) RCB-mediated chlorophagy caused by oversupply of nitrogen suppresses phosphate-starvation stress in plants. Plant Physiol **185**: 318–330

Yuan L, Loqué D, Kojima S, Rauch S, Ishiyama K, Inoue E, Takahashi H, Von Wirén N (2007) The

organization of high-affinity ammonium uptake in Arabidopsis roots depends on the spatial arrangement and biochemical properties of AMT1-type transporters. Plant Cell **19**: 2636–2652

Yuen CCY, Christopher DA (2013) The group IV-A cyclic nucleotide-gated channels, CNGC19 and CNGC20, localize to the vacuole membrane in Arabidopsis thaliana. AoB Plants **5**: 1–14

Zhang G Bin, Yi HY, Gong JM (2014) The Arabidopsis Ethylene/Jasmonic acid-NRT signaling module coordinates nitrate reallocation and the trade-off between growth and environmental adaptation. Plant Cell **26**: 3984–3998

Zhao C, Zhang H, Song C, Zhu J-K, Shabala S (2020) Mechanisms of Plant Responses and Adaptation to Soil Salinity. Innov **1**: 100017

Zhao S, Zhang M, Wang Y (2016) Phosphorylation of ARF2 Relieves Its Repression of Transcription of the K + Transporter Gene HAK5 in Response to Low Potassium Stress. Plant Cell **28**: 3005–3019

Zheng S, Pan T, Fan L, Qiu Q (2013) A Novel AtKEA Gene Family , Homolog of Bacterial K+/ H+ Antiporters , Plays Potential Roles in K + Homeostasis and Osmotic Adjustment in Arabidopsis. PLoS One **8**: e81463

Ziegler G, Terauchi A, Becker A, Armstrong P, Hudson K, Baxter I (2013) Ionomic Screening of Field-Grown Soybean Identifies Mutants with Altered Seed Elemental Composition. Plant Genome **6**: 0

Zioni A BEN, Vaadia Y, Lips SH (1971) Nitrate Uptake by Roots as Regulated by Nitrate Reduction Products of the Shoot. Physiol Plant **24**: 288–290

Figures

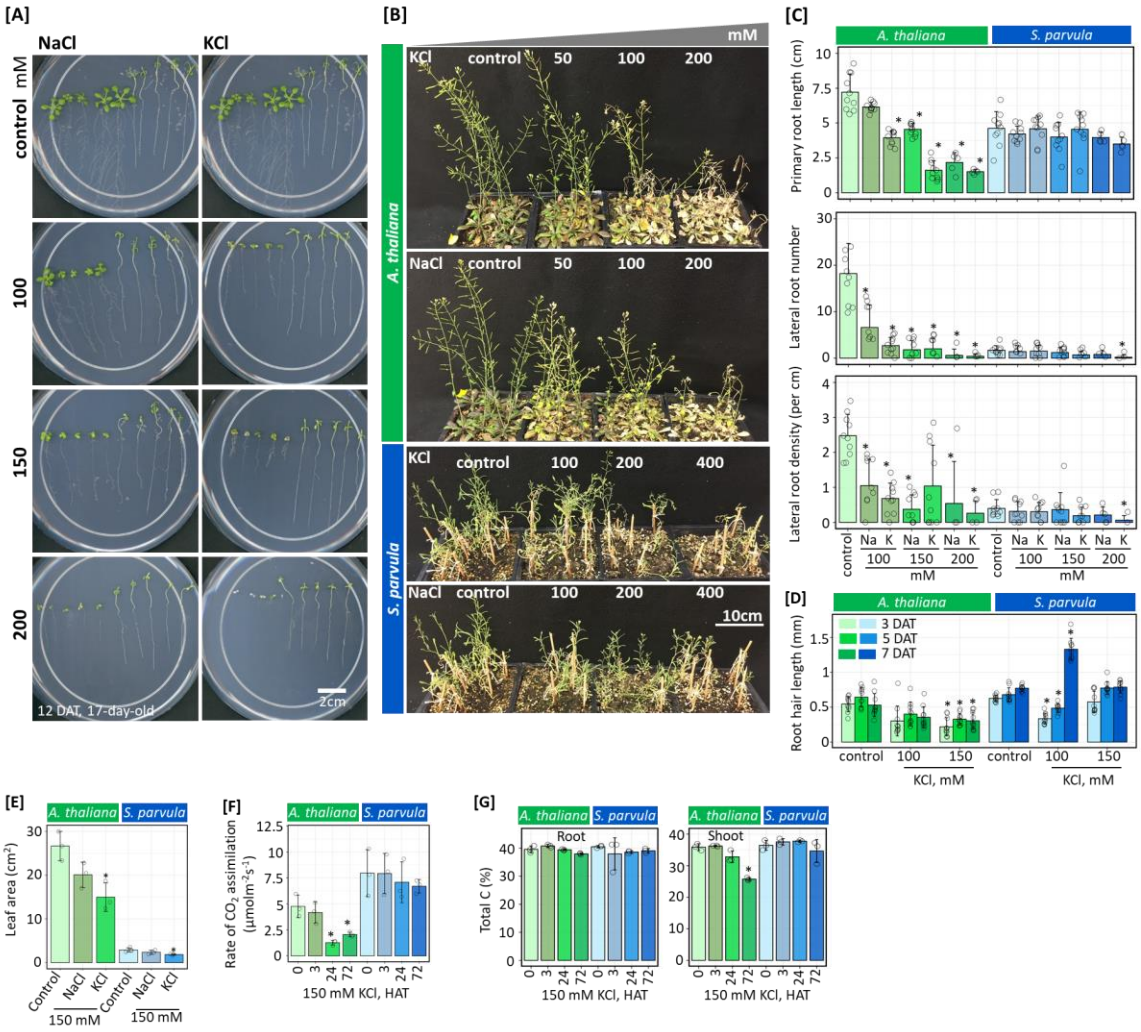

Figure 1. KCl is more toxic than NaCl at the same osmotic strength. [A] Seedlings of *Arabidopsis thaliana* and *Schrenkiella parvula* on 1/4 MS media supplemented with 0 to 200 mM NaCl and KCl. **[B]** 3-week-old plants treated with increasing levels of NaCl and KCl for 2-weeks and imaged after completion of the salt treatment. **[C]** Primary root length, lateral root number, and lateral root density measured on 17-day-old seedlings grown under conditions used in [A] based on a 12-day treatment of NaCl or KCl. **[D]** Root hair length measured under the same growth conditions used in [A] and [D] for variable KCl treatments and monitored for a week. **[E]** Leaf area measured for 5- and 6-week-old hydroponically grown *A. thaliana* and *S. parvula* treated with increasing levels of NaCl and KCl for 1- and 3-weeks. **[F]** Photosynthesis measured as the rate of CO_2 assimilation of the entire shoot/rosette in 25-day-old hydroponically grown plants and monitored up to 72 HAT. **[G]** Total carbon as a % weight based on total dry mass for root and shoot tissue under conditions used in [F]. Minimum 5 plants per condition used in C and D and a minimum of 3 plants per condition used for E and F. Asterisks indicate significant changes between the treated samples to its respective control samples (t-test with $p < 0.05$). Data are presented as mean of at least 3 independent biological replicates ± SD. DAT-Days after treatment, HAT- Hours after treatment.

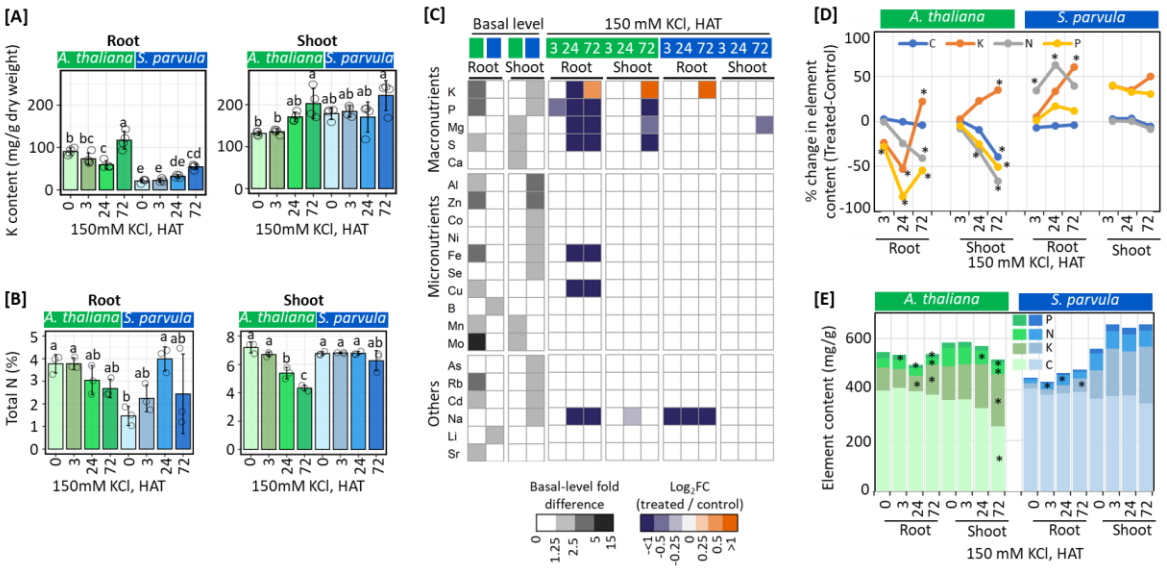

Figure 2. Excess K accumulation caused severe nutrient imbalance in *A. thaliana* compared to *S. parvula*. **[A]** K accumulated differently between *A. thaliana* and *S. parvula*. *A. thaliana* promoted shoot retention while *S. parvula* promoted root retention of K. **[B]** Increased accumulation of K resulted in N depletion in *A. thaliana* compared to *S. parvula*. **[C]** Differential accumulation of K caused imbalances of multiple nutrients in *A. thaliana* roots even in early time points and caused hardly any noticeable differences in *S. parvula*. **[D]** Percent change in CNPK elemental content in root and shoot of *A. thaliana* and *S. parvula* under high [K^+]. *A. thaliana* fails to maintain major macronutrient levels preventing depletion of those pools contrasted to *S. parvula*. **[E]** Total CNPK content in roots and shoots. Data are represented as mean of at least 4 (for A and C) and 3 (for B) independent replicates with ± SD given using ≥ 5 hydroponically grown plants per replicate. Elemental compositions were quantified using ICP-MS and total N was obtained using an elemental combustion system. The total elemental composition is reported after normalization for dry weight. All quantitative measurements were evaluated by one-way ANOVA followed by Tukey's post-hoc test*, p-value* <0.05 and same letters in the bar graph does not differ statistically significantly and asterisks indicate significant changes between the treated samples to its respective control samples. HAT- Hours after treatment.

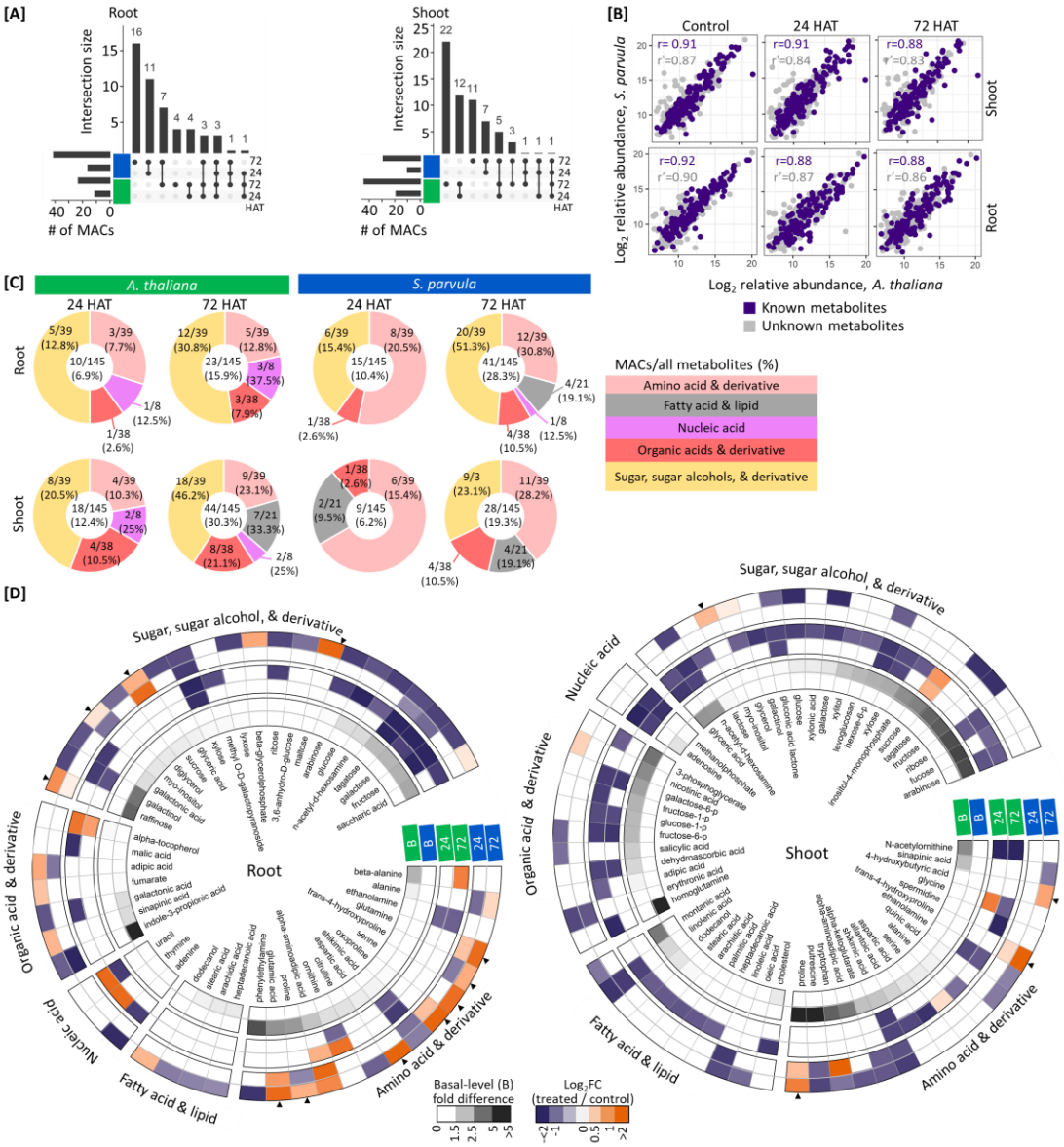

Figure 3. *S. parvula* root metabolome is more responsive than *A. thaliana* and induces specific antioxidants and osmoprotectants to adapt to high K^+ stress in both roots and shoots. **[A]** Metabolites that significantly changed in abundance at 24 and 72 hours after treatment (HAT). **[B]** *A. thaliana* and *S. parvula* metabolome profiles are highly corelated with each other upon high K^+ in both roots and shoots. Pearson correlation coefficient is calculated for 145 known metabolites (r) and all metabolites including the unannotated metabolites (r'). **[C]** Overview of the temporal changes in primary metabolic pools based on known metabolite annotations. Metabolites that significantly changed in abundance at respective time points are shown followed by a "/" and the total number of metabolites counted in that category. **[D]** Individual metabolites in each functional group mapped to represent their abundance starting at basal level (inner circles) to 24 and 72 h of exposure to high K shown in concentric outer rings. Metabolites mostly highlighted in Results and Discussion are marked with arrow heads in the outer circle in both plots. Significance test for metabolite abundance was performed with one-way ANOVA followed by Tukey's post-hoc test, *p-value* <0.05. Data are represented as mean of at least 3 independent replicates ± SD given using ≥ 5 hydroponically grown plants per replicate.

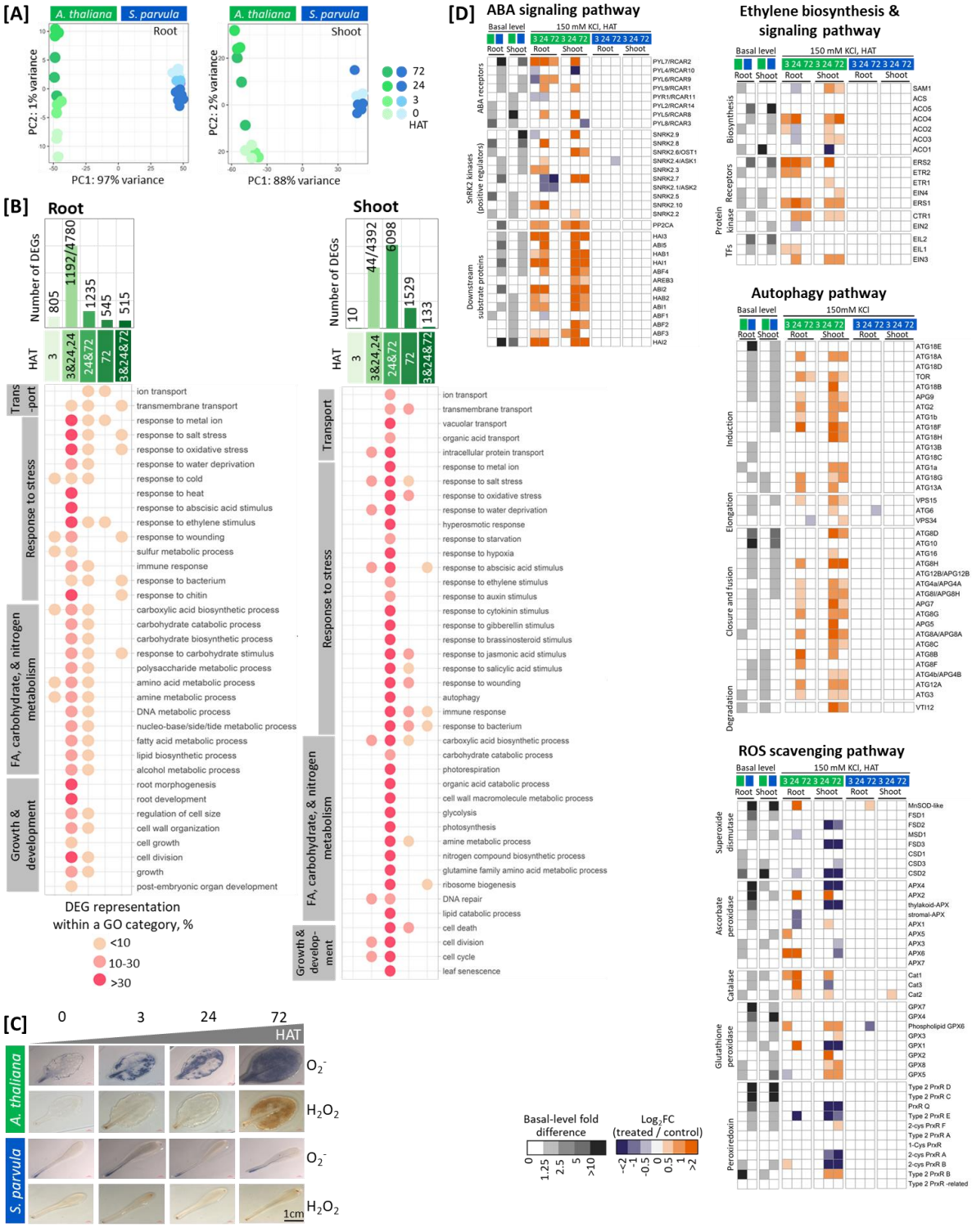

Figure 4. *A. thaliana* shows non-selective transcriptional modifications during excess K^+ stress than *S. parvula*. [A] Principal component analysis (PCA) of ortholog expression between *A. thaliana* and *S. parvula* root and shoot transcriptomes at 0, 3, 24, and 72 hours after treatment (HAT). **[B]** Enriched functional processes based on GO annotations associated with differently expressed genes (DEGs) in *A. thaliana*. The temporal sequence of enriched functions is given as 3 h specific, 3 and 24 h together with 24 h specific, and 72 h, 72 h specific, and present at all-time points from 3-24-72 h. Only functional processes that were detected at least in two time points are shown and the processes are sorted based on their functional hierarchy when applicable. **[C]** *A. thaliana* accumulated higher levels of hydrogen peroxide (H_2O_2) and superoxide ions (O_2^-) in leaves under excess K^+ stress compared to *S. parvula*. Hydroponically grown plants were used treated similar to the plants used for the RNA-Seq study and stained with DAB and NBT. **[D]** Transcriptional profiles of selected pathways that serve as indicators of transcriptional mismanagement in *A. thaliana* during excess K^+ stress compared to *S. parvula*. DEGs were called using DESeq2 with a p-adj value based on Benjamini-Hochberg correction for multiple testing set to <0.01.

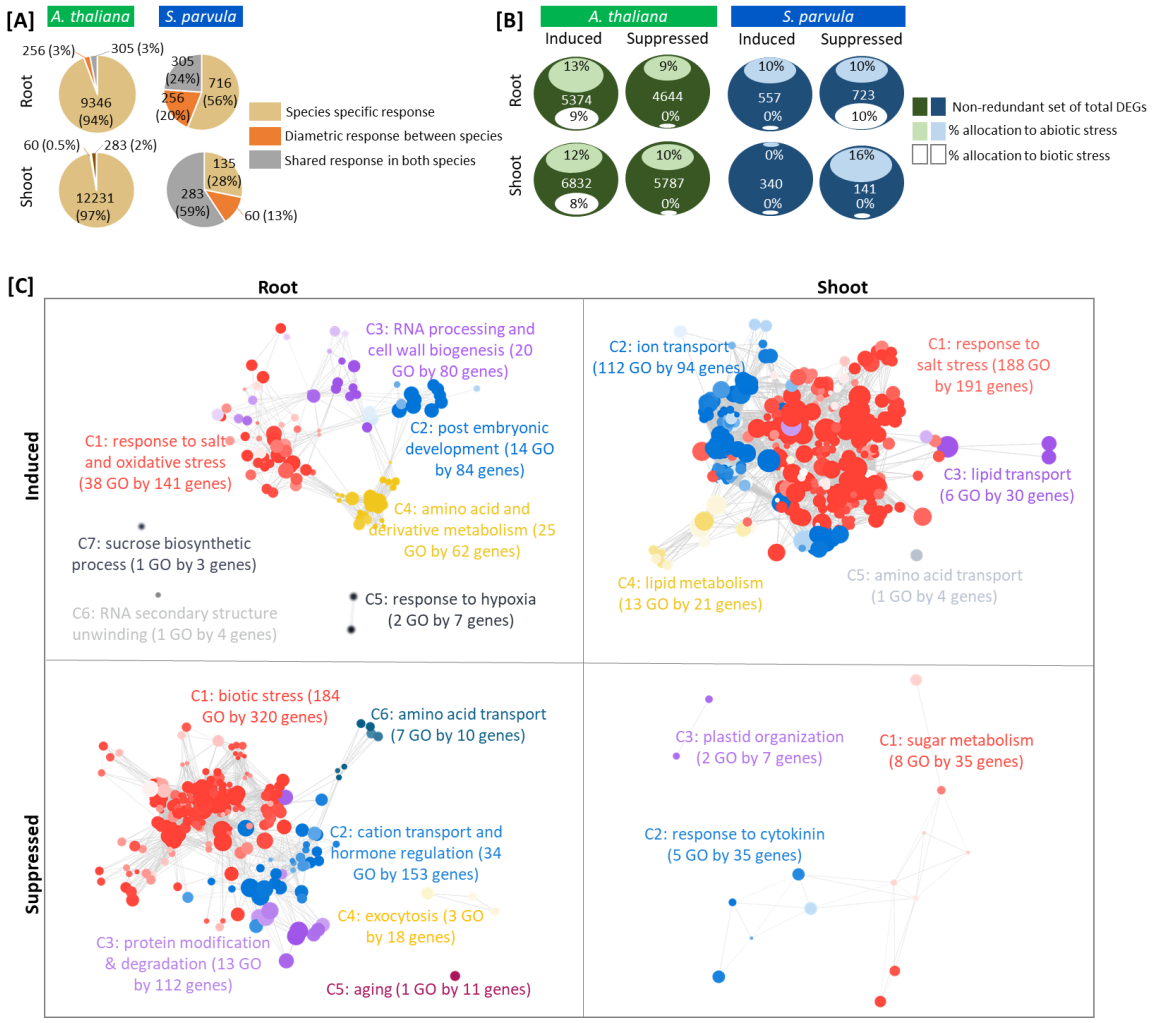

Figure 5. *S. parvula* shows a confined transcriptomic response geared toward concurrent induction of abiotic stress responses and enhanced transcriptional allocation to C and N metabolism. [A] The overall expression specificity and response direction of orthologs in *A. thaliana* and *S. parvula.* Selected orthologs are differentially expressed genes (DEGs) at least in one time point compared to the respective control condition and then counted as a non-redundant set when all 3, 24, and 72 HAT samples were considered for total counts. **[B]** The proportion contributing to abiotic and biotic stress stimuli within non-redundant DEGs. The effort to suppress biotic stress responses in *S. parvula* roots (10%) was similar to the proportional induction for biotic stress responses in *A. thaliana* (9%). **[C]** The functionally enriched processes represented by DEGs in *S. parvula* that responded to high K^+. A non-redundant set from all time points (3, 24, and 72 HAT) are given. A node in each cluster represents a gene ontology (GO) term; size of a node represents the number of genes included in that GO term; the clusters that represent similar functions share the same color and are given a representative cluster name and ID; and the edges between nodes show the DEGs that are shared between functions. All clusters included in the network have adj p-values <0.05 with false discovery rate correction applied. More significant values are represented by darker node colors. The functional enrichment network was created using GOMCL. DEGs were called using DESeq2 with a p-adj value based on Benjamini-Hochberg correction for multiple testing set to <0.01.

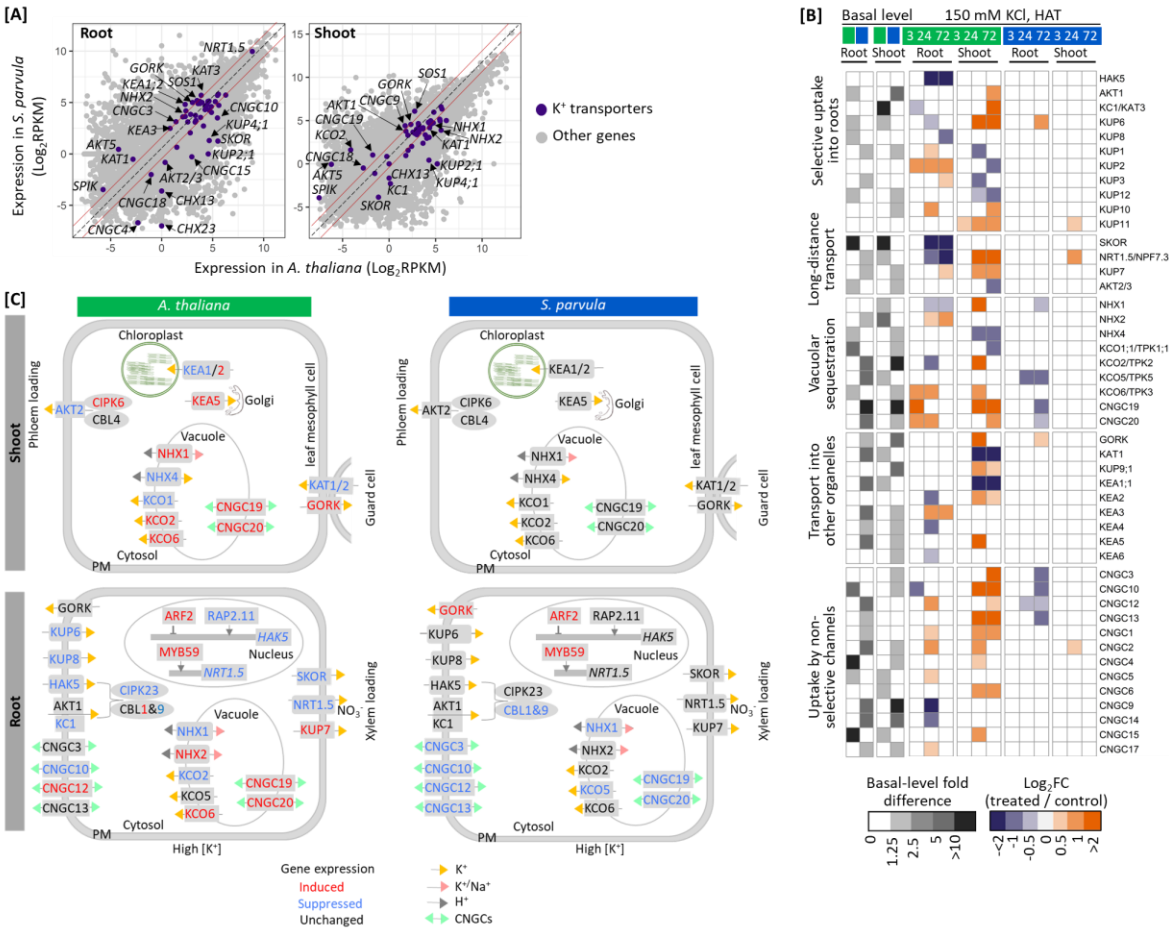

Figure 6. Differential expression of K⁺ transporters in *A. thaliana* and *S. parvula*. [A] Basal level expression comparison of orthologs between *A. thaliana* and *S. parvula* in roots and shoots. The dash-gray diagonal line marks identical expression in both species and solid red lines represent a 2-fold change in one species compared to the other species. Transporters/channels with >2-fold change basal differences between the species are labeled. **[B]** The temporal expression of functionally established K⁺ transporters and channels in *A. thaliana* and their *S. parvula* orthologs upon high K⁺ treatment. **[C]** Key K⁺ transporters and channels differently regulated between roots and shoots in *A. thaliana* and *S. parvula*. DEGs at each time point were called using DESeq2 compared to 0 h with a p-adj value based on Benjamini-Hochberg correction for multiple testing set to <0.01.

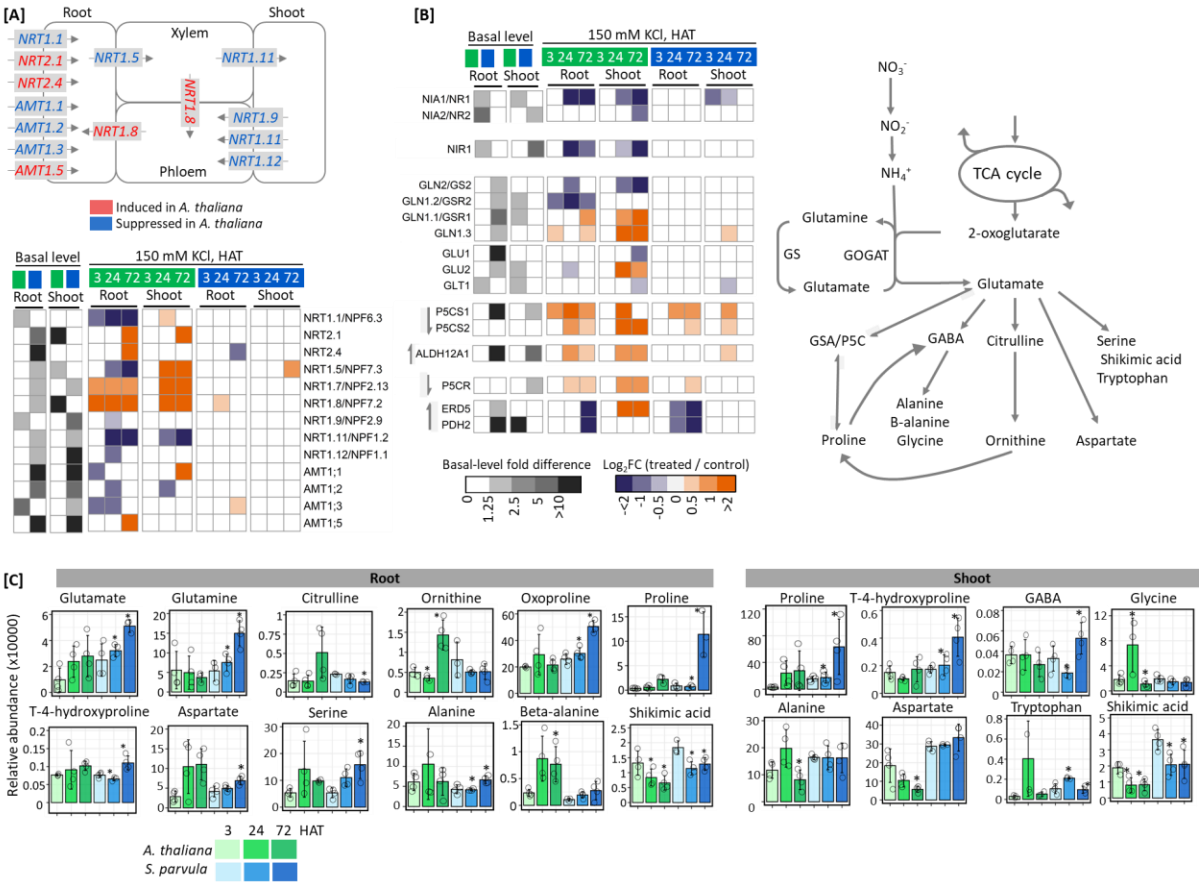

Figure 7. Excess K^+ induced nitrogen starvation and suppressed associated N-assimilation pathways in *A. thaliana* compared to *S. parvula*. **[A]** Nitrogen uptake and distribution was severely affected in *A. thaliana* upon high K^+. The expression changes associated with major nitrogen transporters in *A. thaliana* that regulate root uptake and long-distance transport of N are summarized. **[B]** Coordinated transcriptional regulation showing high K^+-induced suppression of nitrogen assimilation and efforts to accumulate glutamate-derived osmoprotectants. The arrows in front of heatmap blocks indicate the direction of the reaction. **[C]** The primary metabolite pools derived from glutamate in roots and shoots. DEGs at each time point were called using DESeq2 compared to 0 h with a p-adj value based on Benjamini-Hochberg correction for multiple testing set to <0.01. Significance test for metabolite abundances was performed with one-way ANOVA followed by Tukey's post-hoc test, *p-value* <0.05. Data are represented as mean of at least 3 independent replicates ± SD (≥ 5 hydroponically grown plants per replicate).

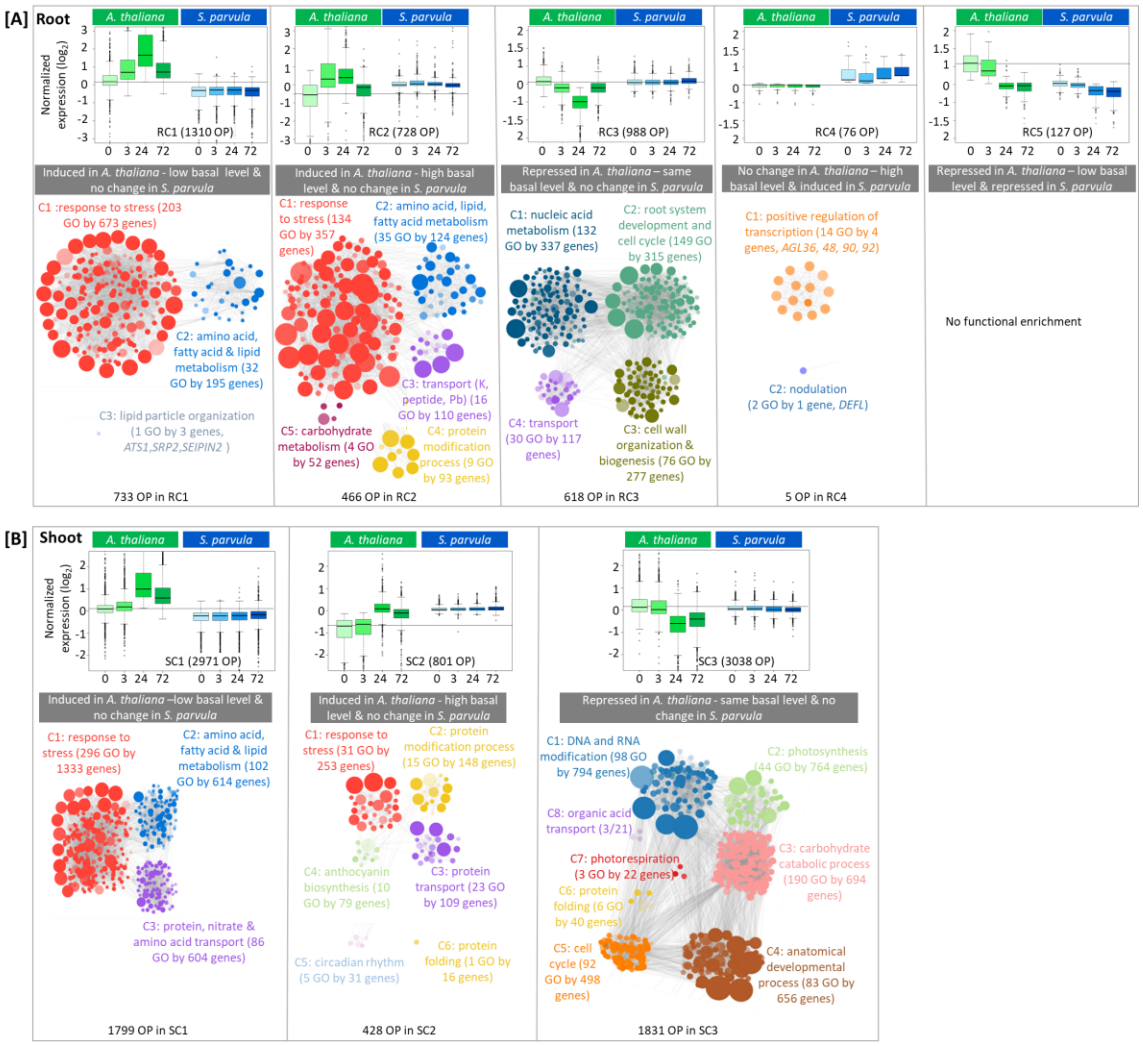

Figure 8. Co-expressed ortholog gene modules highlight stress preparedness towards high K^+ stress in *S. parvula* orthologs that are constitutively expressed compared to induction or suppression of orthologs in *A. thaliana*. Normalized gene expression clusters of ortholog pairs (OP) between *A. thaliana* and *S. parvula* in **[A]** roots and **[B]** shoots. Fuzzy K-means clustering was used to find temporally co-regulated clusters with a membership cutoff of ≤0.5. Box and whisker plots mark the median expression at each time point with the thick line within the box; interquartile range between first and third quartile are shown with the box; and interquartile range x 1.5 are marked by whiskers for lower and upper extremes. Basal level for 0 h in *A. thaliana* is marked by a grey line in all plots. Each cluster was used for a functional enrichment analysis represented by GOMCL summaries placed below co-expression plots. A node in each cluster represents a gene ontology (GO) term; size of a node represents the number of genes included in that GO term; the clusters that represent similar functions share the same color and are given a representative cluster name and the edges between nodes show the orthologs that are shared between functions. All clusters included in the network have adj p-values <0.05 with false discovery rate correction applied. More significant values are represented by darker nodes.

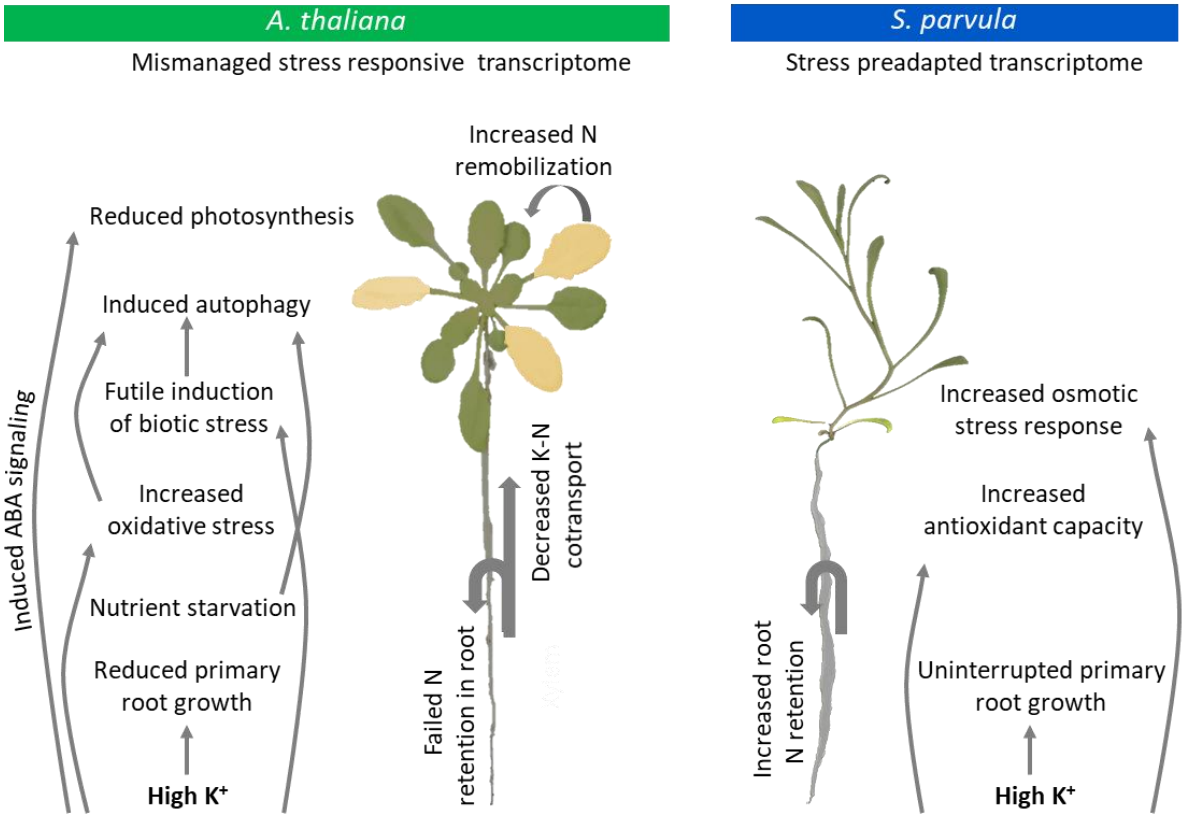

Figure 9. Deterministic cellular processes in surviving high K^+ stress.

Supplementary figures

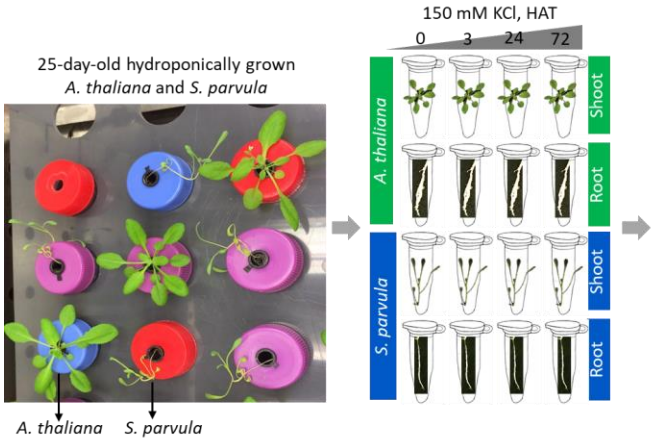

Experiment	# replicates per condition	Total number of samples
Ionome	4	64
Transcriptome	3	48
Metabolome	4	48

Figure S1. Sampling scheme for the ionome, metabolome, and transcriptome experiments performed in this study. 25-day-old *Arabidopsis thaliana* and *Schrenkiella parvula* plants were grown in 1/5th Hoagland's solution with/without 150 mM KCl for up to 72 hours after treatment (HAT). All samples were 28-day-old at the time of sample harvest. Both ionome and metabolome profiles have 4 biological replicates and transcriptome samples have 3 biological replicates. Each replicate contains tissues from at least 5 different plants.

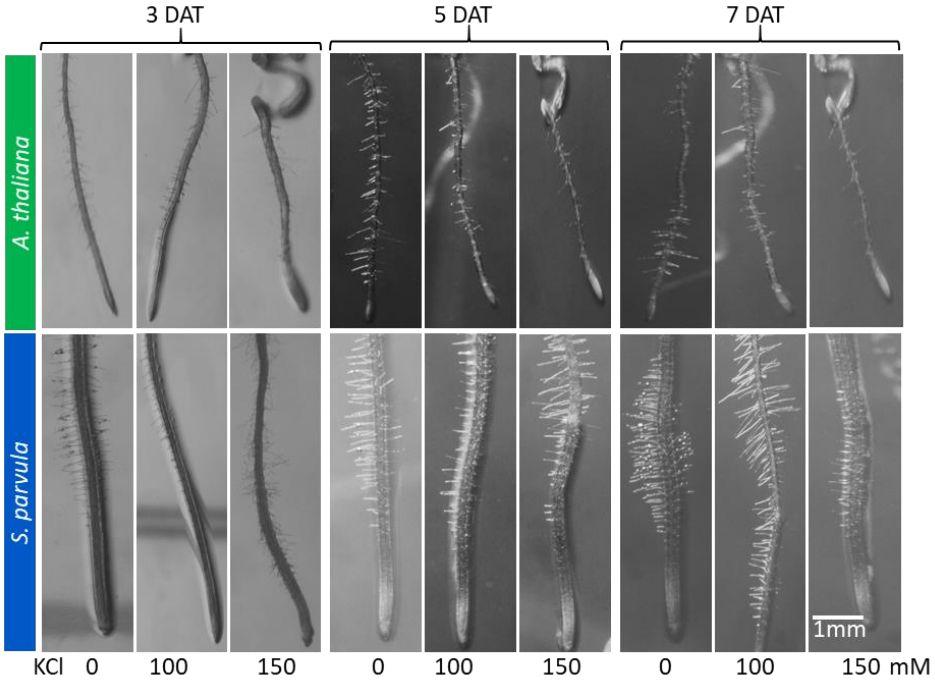

Figure S2. Representative images showing the effect of KCl on root hair growth in *A. thaliana* and *S. parvula*. Scale bars are 1 mm for all the panels. Seeds were germinated in 1/4th MS and transferred to the corresponding plates with 100 or 150 mM KCl 5 days after germination. Same roots were photographed on 3, 5, and 7 DAT. DAT- Days after treatment.

[A]

A. thaliana

Root

Enriched processes	Total # of metabolites	# of MACs*	P-value	P-adj
Galactose Metabolism	38	4	0.004	0.411
Lactose Degradation	9	2	0.011	0.533

Shoot

Enriched processes	Total # of metabolites	# of MACs*	P-value	P-adj
Galactose Metabolism	38	7	0.0003	0.025
Lactose Degradation	9	3	0.003	0.154
Glycerolipid Metabolism	25	4	0.011	0.26
Glycolysis	25	4	0.011	0.26
Lactose Synthesis	20	3	0.032	0.553
Gluconeogenesis	35	4	0.034	0.553

S. parvula

Root

Enriched processes	Total # of metabolites	# of MACs*	P-value	P-adj
Galactose Metabolism	38	7	0.0002	0.016
Urea Cycle	29	6	0.0003	0.016
Aspartate Metabolism	35	5	0.006	0.199
Glucose-Alanine Cycle	13	3	0.009	0.22
Ammonia Recycling	32	4	0.023	0.449
Arginine and Proline Metabolism	53	5	0.034	0.519
Lactose Degradation	9	2	0.037	0.519
Malate-Aspartate Shuttle	10	2	0.045	0.555

Shoot

Enriched processes	Total # of metabolites	# of MACs*	P-value	P-adj
Galactose Metabolism	38	5	0.002	0.196
Lactose Degradation	9	2	0.02	0.981
Glucose-Alanine Cycle	13	2	0.041	1

Significantly enriched process

*Metabolites that significantly changed in abundance

[B]

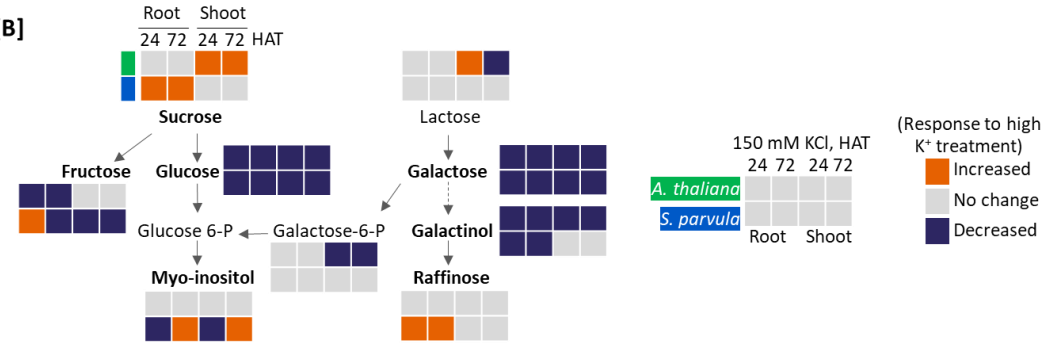

Figure S3. Carbohydrate and nitrogen metabolism related processes were enriched in *S. parvula* roots. **[A]** Enriched metabolic pathways in *A. thaliana* and *S. parvula* in response to excess K stress. Metabolite Enrichment Analysis was performed with MetaboAnalyst with a p-adj cut off set to < 0.05. p-values were adjusted using Benjamini-Hochberg correction for multiple testing. **[B]** Simplified galactose metabolism pathway. The seven metabolites that significantly changed in abundance and quantified using GC-MS are indicated in bold font.

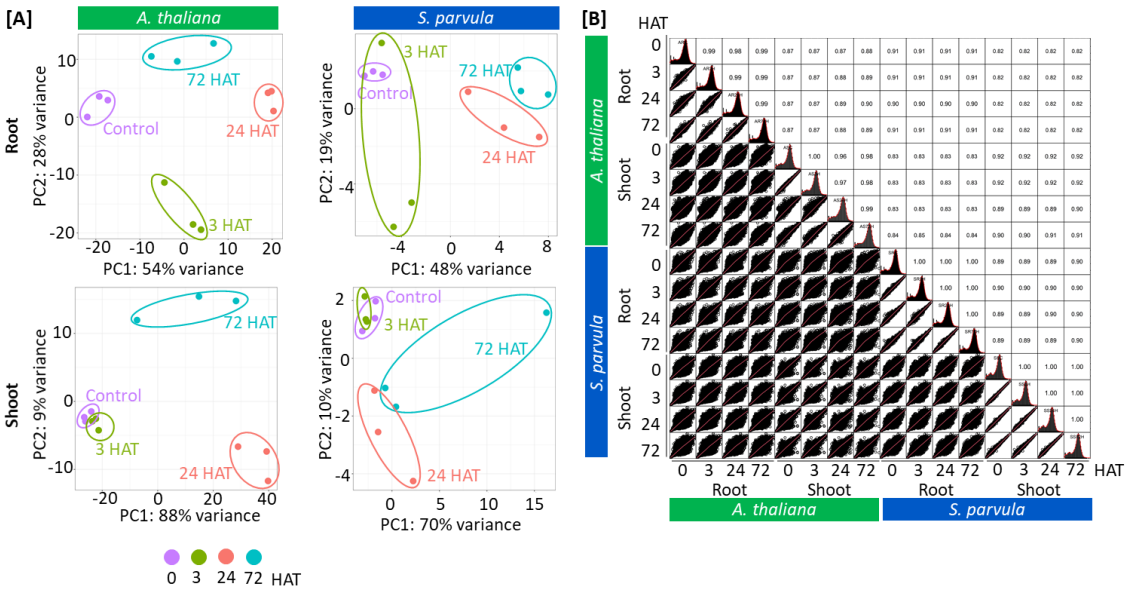

Figure S4. **Overview of transcriptomes in each condition tested in response to high K stress in *A. thaliana* and *S. parvula* roots. [A]** Principal component analysis (PCA) for 0, 3, 24, and 72 hours after treatment (HAT) for *A. thaliana* (left panel) and *S. parvula* roots and shoots. **[B]** Overall transcript level correlation between conditions. Correlation plots were generated using PerformanceAnalytics library in R 4.0.2. Pearson correlation coefficient is given within plots for each comparison.

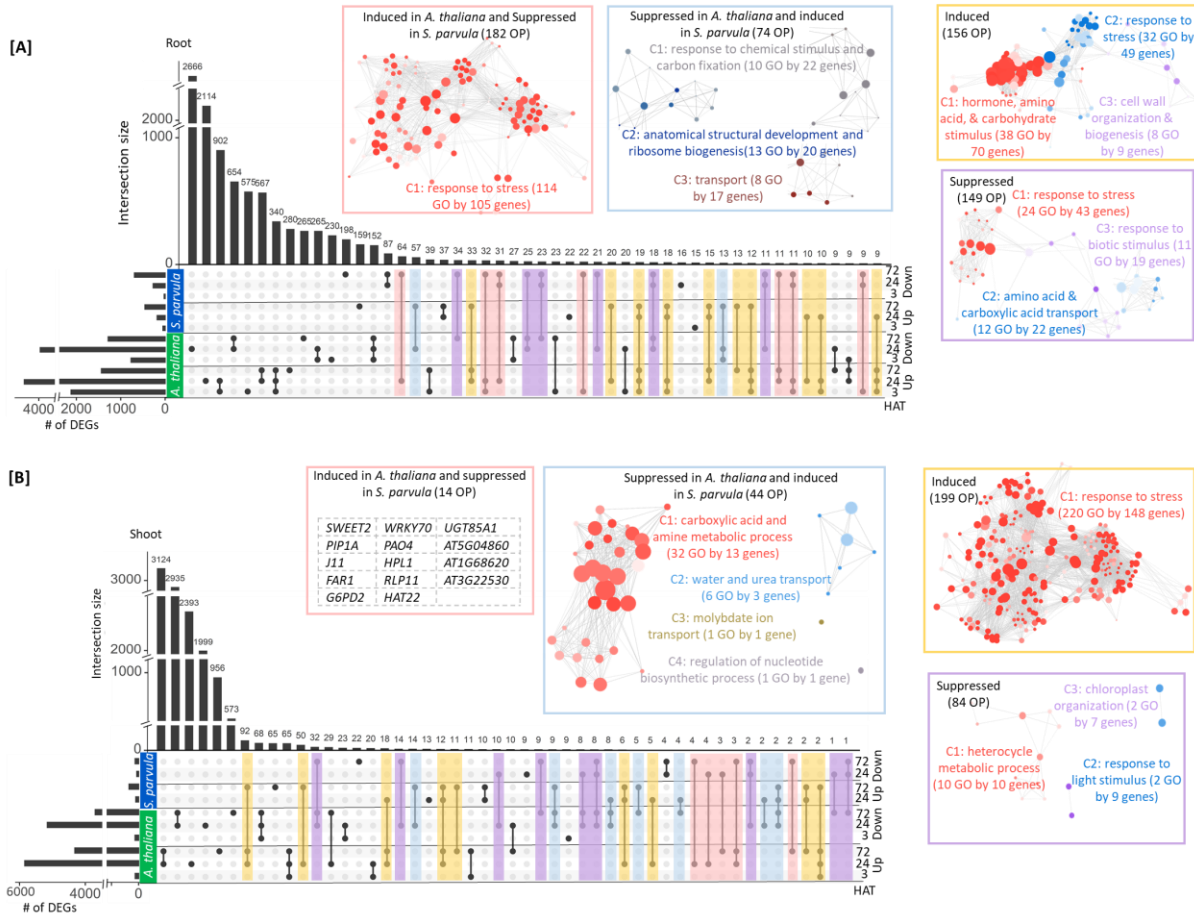

Figure S5. **The majority of differentially expressed genes (DEGs) show species specific responses followed by tissue and response time specificity.** Differentially expressed genes (DEGs) between *A. thaliana* and *S. parvula* for **[A]** roots and **[B]** shoots. Enriched functions are highlighted for diametric and shared responses between differently regulated ortholog pairs (OP). DEGs at each time point were called using DESeq2 compared to 0 h with a p-adj value based on Benjamini-Hochberg correction for multiple testing set to <0.01. The shared genes were plotted using UpsetR in R 4.0.2.

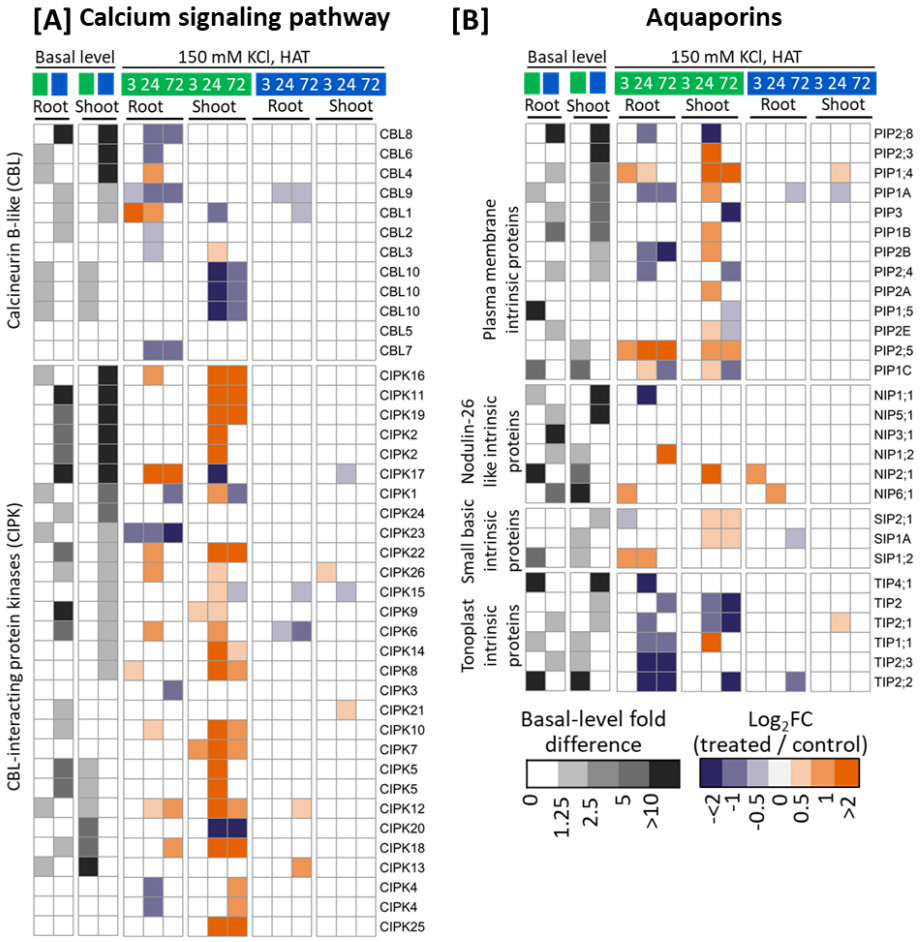

Figure S6. Genes coding for calcium signaling and aquaporins are differently regulated during high K^+ stress. Genes associated with **[A]** calcium signaling pathway and **[B]** aquaporins during high K^+ in root and shoot of *A. thaliana* and *S. parvula*. The significantly changed genes at least in one condition are presented in the heatmap. DEGs at each time point were called using DESeq2 compared to 0 h with a p-adj value based on Benjamini-Hochberg correction for multiple testing set to <0.01.

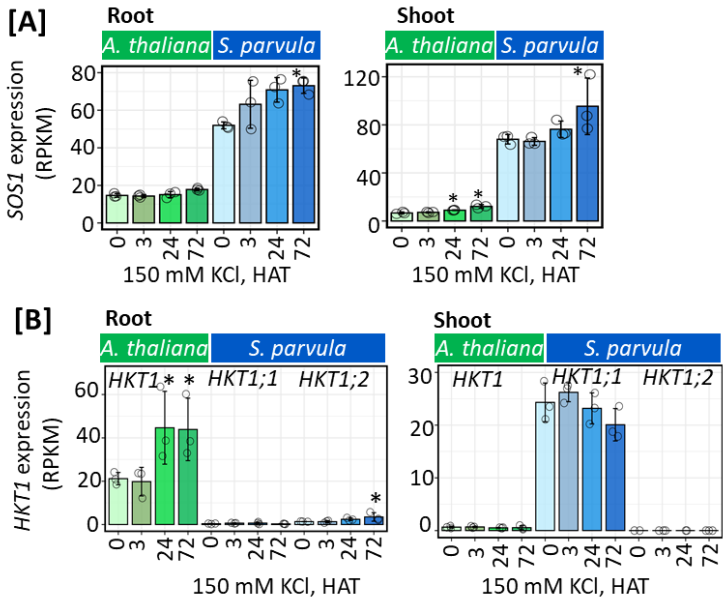

Figure S7. Normalized expression of [A] *SOS1* and [B] *HKT1* in roots and shoots of *A. thaliana* and *S. parvula* under 150 mM KCl treatments. *HKT1* has undergone a tandem duplication in *S. parvula,* and *SpHKT1;2* is known to function in selective K^+ transport. *AtHKT1* and *SpHKT1;1* are selective Na transporters. * represent DEGs at each time point called using DESeq2 compared to 0 h with a p-adj value based on Benjamini-Hochberg correction for multiple testing set to <0.01.